



UV/ozone irradiation manipulates immune response for antibacterial activity and bone regeneration on titanium

Yuan Yuan Yang^a, Honghao Zhang^{a,*}, Satoshi Komasa^a, Yukihiro Morimoto^b, Tohru Sekino^b, Takayoshi Kawazoe^c, Joji Okazaki^a

^a Department of Removable Prosthodontics and Occlusion, Osaka Dental University, 8-1 Kuzuha-hanazono-cho, Hirakata, Osaka 573-1121, Japan

^b The Institute of Scientific and Industrial Research, Osaka University, Suita, Osaka 565-0871, Japan

^c Osaka Dental University, 8-1 Kuzuha-hanazono-cho, Hirakata, Osaka 573-1121, Japan

ARTICLE INFO

Keywords:

Immune response
UV/ozone irradiation
Immunomodulatory antibacterial
Osteoimmunomodulation

ABSTRACT

The immunomodulatory antibacterial activity and osteoimmunomodulatory properties of implantable bio-materials significantly influence bone regeneration. Various types of ultraviolet (UV) instrument are currently in use to greatly enhance the antibacterial activity and osteoconductive capability of titanium, it remains unclear how UV treatment modulates immune response. Compared to traditional UV treatment, the combination of low-dose ozone with UV irradiation is considered a new option to give benefits to surface modification and reduce the drawbacks of UV and ozone individually. Herein, the aim of this study was to elucidate the immune-modulatory properties of macrophages on UV/ozone-irradiated titanium that serve as defense against *S. aureus* and the crosstalk between immune cells and osteoblasts. Three different cell and bacteria co-culture systems were developed in order to investigate the race between host cells and bacteria to occupy the surface. *In vitro* immunological experiments indicated that UV/ozone irradiation significantly enhanced the phagocytic and bactericidal activity of macrophages against *S. aureus*. Further, *in vitro* and *in vivo* studies evidenced the favorable osteoimmune environment for osteogenic differentiation and bone formation. This research suggests vital therapeutic potential of UV/ozone irradiation for preventing the biomaterial-associated infections and achieving favorable bone formation simultaneously.

1. Introduction

Biomaterial-associated infections and insufficient osteogenesis are two frequent and severe complications that lead to osteomyelitis and bone fracture nonunion [1–3]. The host immune defenses not only react against bacteria that contaminate the biomaterial, but also play crucial roles in recruitment and differentiation of mesenchymal stem cells (MSC) [4,5]. Race between host cells and bacteria to occupy the biomaterials surfaces is considered to largely determine the fate of bone formation [2]. Furthermore, in implant-associated infections, biofilm can greatly attenuate host immune cells and allow bacteria to persist in the host environment [6]. Therefore, in addition to the direct antibacterial activity, ideal biomaterials should enhance local innate immunity against bacteria and rapid integration of host tissues. Current research on antibacterial activity and cell-based bone tissue formation has largely focused on utilizing bacteria or MSC individually. In contrast, relatively little research has focused on the immune cells-bacteria or MSC

crosstalk, despite them being essential for developing smart biomaterials with both excellent antibacterial and osteogenic activity for clinical applications.

Owing to their exogenous nature, biomaterials used in implantable medical devices are recognized by immune system as foreign bodies and immediately evoke the host innate immune response upon implantation [7]. Inappropriate development of a foreign body reaction (FBR) might result in fibrous capsulation surrounding the implanted biomaterial, impeding its integration with bone tissues [8,9]. Among the innate immunity components, macrophages are sentinel cells that are long-lived, require vesicular trafficking events, and produce high levels of proinflammatory mediators to orchestrate the elimination of bacteria [10,11]. Macrophages are phagocytic cells capable of ingesting and destroying invading organisms. They can also present microbial antigens on their surface for eliciting acquired immune responses [12]. In addition to fighting bacterial infections, resident tissue macrophages are involved in removing dead cells, cellular debris, and toxic materials

* Corresponding author.

E-mail addresses: yangyuan0801@outlook.com (Y. Yang), joecheung_asuka@hotmail.com (H. Zhang).

<https://doi.org/10.1016/j.msec.2021.112377>

Received 28 May 2021; Received in revised form 10 August 2021; Accepted 13 August 2021

Available online 14 August 2021

0928-4931/© 2021 Elsevier B.V. All rights reserved.

[13,14]. However, biofilm formation on biomaterials can cause dormancy in the host immune response by preventing phagocytosis and inflammation of immune cells, leading to massive bone resorption [15,16]. *Staphylococcus aureus*, which is the leading cause of pathogen-related implant infections, has multiple mechanisms for attachment and biofilm formation and has high rates of antibiotic resistance [17,18]. Although macrophages are highly effective at killing most bacteria, *S. aureus* evade destruction by the immune system to survive and cause chronic implant infections. An enhanced understanding of the molecular mechanisms of biomaterial-modulated macrophage response against *S. aureus* is essential for developing new smart biomaterials for preventing or curing chronic implant-infections.

Osteoimmunology investigates the dynamic reciprocal interactions between immune and bone cells, emphasizing the close relationship between immune and myeloid lineage cells, including shared cytokines, chemokines, and transcription factors [19–21]. Bone formation is a dynamic process that continuously undergoes coupled resorption and formation mediated by immune cells (bone remodeling), which is required to maintain bone homeostasis in humans [22]. Advanced biomaterials implant should provide an adequate immune response that can induce beneficial osteogenesis over osteoclastogenesis for functional bone regeneration [19,23]. Macrophages, among the first immune cells to arrive at bone fracture sites, are essentially associated with the early stage of inflammation, chondrogenesis, and deposition of woven bone in bone fracture [24,25]. Importantly, the functional dynamic plasticity of macrophages renders them highly attractive targets for immunomodulation. This includes M1 macrophages, which enhance inflammation and produce pro-inflammation cytokines, such as IL-6 and TNF, and M2 macrophages, which suppress inflammation by secreting anti-inflammation cytokines and improve tissue regeneration by secreting tissue repair signals, including IL-10, BMP-2, and VEGF [13,26]. Macrophages can rapidly change their phenotype in response to local microenvironmental signals. Both M1 and M2 macrophages play important roles in osteogenic differentiation. Specifically, M1 macrophages contribute to osteogenesis in the early and middle stage without enhancing matrix mineralization, while M2 macrophages contribute to matrix mineralization during later stage of fracture healing [27]. However, an excessive and prolonged M1-mediated inflammatory response frequently occurs during the bone healing process, particularly in patients with chronic systemic inflammation (known as “inflammaging”), which may result in delayed bone regeneration or bone destruction [28–30]. Thus, biomaterials that promote M2 macrophage phenotype modulation are important for optimal bone formation.

The surface physicochemical properties of biomaterials are crucial in modulating antibacterial activity and cellular behaviors [31,32]. In particular, metal nanoparticles applied to a biomaterial surface increased its osteogenic functions and antibacterial ability; however, cellular toxicity of the metal nanoparticles limited their clinical application [33–35]. In contrast, UV treatment of titanium and titanium-alloy implants has been widely used for orthopedic and dental implants in clinical surgeries due to its ability to greatly enhance titanium's antibacterial activity and osteoconductive capability simultaneously [36–40]. Recently, UV/ozone irradiation is considered to be one of the new methods to improve bioactivity of biomaterial surface. UV/ozone irradiation modifies the hydrophilicity and generate oxygen radicals on the biomaterial surface by UV irradiation in an atmospheric gas containing oxygen. Improving cell behavior on biomaterials by UV/ozone irradiation has been widely studied [40]. However, the effect of UV/ozone irradiated titanium on the innate host response is unclear, and its immunomodulatory antibacterial and osteoimmunomodulatory effects have not been investigated. Herein, the direct and macrophage-induced immunomodulatory antibacterial activity of UV/ozone irradiated titanium were examined using *Staphylococcus aureus* and macrophage co-culture models. Furthermore, we also evaluated the effects of UV/ozone irradiated titanium on the modulation of macrophages and the subsequent osteogenic activity by using rat bone marrow mesenchymal

stem cells (rBMMSC) *in vitro* and rat femurs *in vivo*. We hypothesized that UV/ozone irradiated titanium would have both favorable immunoregulatory antibacterial activity and osteoimmunomodulatory properties with favorable bone formation.

2. Materials and methods

2.1. Sample preparation

Commercial pure titanium discs (diameter, 15 mm; thickness, 1 mm) were polished on one side with abrasive papers (Waterproof Paper® Nos. 800, 1000, and 1500; Riken Corundum Co. Ltd., Saitama, Japan) for use in surface characterization and *in vitro* studies, while pure titanium screw implants (external diameter, 1.2 mm; length, 12 mm) were prepared by mechanical grinding for *in vivo* animal evaluation. All titanium samples were ultrasonically cleaned successively with acetone, ethanol, and deionized water (each for 10 min). All samples were sterilized by dry heat at 160 °C for 3 h. Half of the titanium samples were irradiated with UV light for 12 min (Voltage: AC100V; Operating temperature: 15–30 °C; Wavelength: 172 nm, Illuminance: 10 mW/cm²) immediately prior to use, while the untreated samples were used as controls. The concentration of ozone treatment is 10 ppm. The UV/ozone irradiated titanium is named as Ti-UV and untreated titanium is named as Ti.

2.2. Surface characterization

The surface morphology of the titanium samples was examined by scanning electron microscopy (SEM) (S-4800; Hitachi, Tokyo, Japan). The surface chemical states and elemental composition were determined by X-ray photoelectron spectrometry (XPS; PHI X-tool; ULVAC-PHI, Kanagawa, Japan). The water contact angles on the samples were measured using a contact angle measurement system (VSA2500 XE; AST Products, Billerica, MA, USA) by application of 2 µL ddH₂O to the surface.

2.3. Cell culture

The murine-derived macrophage cell line (RAW264.7) (EC91062702, KAC Co., Kyoto, Japan) and rat bone marrow mesenchymal stem cells (rBMMSC) were used in this study. RAW264.7 cells were maintained in α -minimum essential medium (α -MEM, Nacalai Tesque, Inc., Kyoto, Japan) supplemented with 10% Fetal Bovine Serum (FBS, Sigma-Aldrich, St. Louis, MO, USA) and 1% penicillin/streptomycin and cultured at 37 °C with 5% CO₂. Following this, adherent cells were dislodged by gently passing a cell scraper upon reaching around 80% confluence.

Rat BMMSC were isolated from the femurs of 8-week-old Sprague Dawley rats (Shimizu Laboratory Supplies Co., Kyoto, Japan) as previously described [41] and were maintained in minimum essential medium (MEM, Nacalai Tesque, Inc., Kyoto, Japan), supplemented with 10% FBS and 1% penicillin/streptomycin, and incubated in a humidified incubator (37 °C, 5% CO₂). The medium was replaced every 3 d. The confluent cells were subcultured by trypsinization, and cells at passage 3 were used for subsequent studies.

2.4. Inflammatory response of macrophages

2.4.1. Cell morphology and viability

For SEM analyses, RAW264.7 cells (1×10^5 cells/well) were seeded onto the prepared Ti and Ti-UV samples in a 24-well plate. After culturing for 1 d, the cells were washed thrice with phosphate buffer saline (PBS, pH 7.4, Gibco™, Thermo Fisher Life Technologies Ltd., Tokyo, Japan), fixed with 2% glutaraldehyde for 2 h, and then dehydrated through a series of ethanol concentrations (50%, 60%, 70%, 80%, 90%, 99%, and anhydrous ethanol). The samples were dried in a critical

point dryer (HCP-1; Hitachi, Tokyo, Japan), followed by coating with platinum–palladium by using an ion sputter machine (Ion sputter E-1030; Hitachi) prior to SEM observation (S-4800; Hitachi).

CellTiter Blue® Cell Viability Assay (Promega, Madison, WI, USA) was used to evaluate cell viability. RAW 264.7 cells (5×10^4) were seeded onto Plate, Ti, and Ti-UV of the 24-well plate for 1, 3, 6, or 24 h. The samples were washed twice with PBS and treated with 300 μ L of diluted CellTiter-Blue® Reagent (50 μ L CellTiter-Blue® Reagent diluted in 250 μ L PBS). Finally, after 1 h incubation (37 °C; 5% CO₂), 100 μ L reagent/well was transferred to a 96-well plate and examined by spectrophotometer (SpectraMax M5; Molecular Devices, San Jose, CA, USA) at 560/590 nm.

2.4.2. Polarization of macrophages

To explore the effects of UV/ozone treatment on macrophage phenotype, expression levels of M1 cell surface markers CD11c, were evaluated by flow cytometry. RAW 264.7 cells were seeded onto the samples at a density of 10^5 cells/well for 3 d, then cells were detached by gently scraping. Nonspecific protein binding was blocked by 1% BSA/PBS, followed by staining with CD11c Monoclonal Antibody (eBioscience™, Tokyo, Japan) for 30 min at 4 °C in the dark. Meanwhile, Armenian Hamster IgG Isotype Control (eBio299Arm, Alexa Fluor 488, eBioscience™) were used as isotype controls, and cells untreated were used as unstained control. After washing with 1% BSA/PBS, the cells were analyzed on a FC500 flow cytometer (Beckman Coulter, Brea, CA, USA). The data were analyzed using Flowing Software (www.flowingsoftware.com).

2.4.3. Inflammatory gene expression of macrophages

RAW 264.7 cells were seeded on the Plate, Ti, and Ti-UV in the 24-well plate at a density of 10^5 cells/well. The cells were incubated for 6 d, and the medium was changed on day 3. On days 3 and 6, the conditioned media were collected and centrifuged (1500 rpm at 4 °C) to obtain the supernatants. The culture medium (MEM containing 10% FBS and 1% penicillin/streptomycin, with or without osteogenic supplements) was mixed with the acquired supernatant at a ratio of 2:1 to obtain the conditioned medium (CM) for further experiments.

The expression levels of inflammation-related genes, M1 phenotype (TNF- α , IL-6) and M2 phenotype (IL-10, Arg-1), were evaluated using a real-time TaqMan reverse transcriptase polymerase chain reaction (RT-qPCR) assay (Life Technologies, Carlsbad, CA, USA). The relative gene expression levels of each group were determined by the $\Delta\Delta C_t$ method and normalized to the house keeping gene, glyceraldehyde 3-phosphate dehydrogenase (GAPDH).

2.4.4. Osteogenic gene expression of macrophages

To investigate the effects of UV/ozone treatment on osteogenic gene expression by RAW 264.7 cells, expression levels of Bone Morphogenetic Protein 6 (BMP-6), transforming growth factor beta 1 (TGF β 1), Vascular endothelial growth factor (VEGF), and Oncostatin M (OSM) were analyzed by RT-qPCR, as described in Section 2.4.3.

2.5. Inflammatory response of lipopolysaccharide (LPS)-activated macrophages

2.5.1. Cell morphology and viability of LPS-activated macrophages

To investigate the acute inflammatory response of macrophage on samples, *E. coli* LPS was used as the inflammation stimulus in our study. RAW 264.7 cells were seeded on the Plate, Ti, and Ti-UV in the 24-well plate at a density of 10^5 cells/well. LPS (20 ng/mL) was added to the culture medium. After overnight incubation with LPS, the culture media of different groups was collected and centrifuged to obtain the supernatants for further experiments. The cell morphology and viability of LPS-activated macrophages was assessed by SEM and CellTiter Blue® Cell Viability Assay as described in Section 2.4.1.

2.5.2. Measurement of mitochondrial membrane potential change and intracellular reactive oxygen species (ROS) level of LPS-activated macrophages

Mitochondrial membrane potential ($\Delta\psi_m$), an important parameter of mitochondrial function, is used as an indicator of cell health. The JC-1 kit (10,009,172, Cayman, Ann Arbor, Michigan, USA) was used to determine the effects of LPS on the mitochondrial membrane potential of macrophages in different samples. Macrophages were washed with PBS three times and incubated in 100 μ L of the JC-1 Staining Solution per mL of culture medium for 30 min at 37 °C. Subsequently, the staining solution was removed and washed thrice with PBS. Cells were visualized and photographed using a confocal laser-scanning microscope (LSM700; Carl Zeiss, Oberkochen, Germany), and images were analyzed using ImageJ software (National Institutes of Health, Bethesda, MD, USA). Healthy cells with mainly JC-1 J-aggregates were detected at excitation/ emission wavelengths of 540/570 nm, respectively, while apoptotic or unhealthy cells with mainly JC-1 monomers were detected at 485/535 nm, respectively.

The intracellular ROS level was determined with CellROX® oxidative stress reagents (C10422, Thermo Fisher Life Technologies Ltd., Tokyo, Japan). The cells were washed with PBS three times and incubated in medium containing 5 μ M CellROX® oxidative stress reagents for 30 min at 37 °C. Following this, the cells were collected by trypsinization and transferred to a 96-well plate. The ROS level was examined by a spectrophotometer (SpectraMax M5; Molecular Devices, San Jose, CA, USA). The intracellular ROS level was normalized against the total cell count by dividing by the total amount of DNA in each well, which was determined using the PicoGreen dsDNA assay kit (Thermo Fisher Life Technologies Ltd., Tokyo, Japan).

2.5.3. Inflammatory gene expression of LPS-activated macrophages

The expression levels of inflammation-related genes, M1 phenotype (TNF- α , IL-6) and M2 phenotype (IL-10, Arg-1), in macrophages under the same treatments as previously described were detected by RT-PCR.

2.5.4. Osteogenic gene expression of LPS-activated macrophages

The expression levels of BMP-6, transforming growth factor beta 1 (TGF β 1), Vascular endothelial growth factor (VEGF), and OSM were analyzed by RT-qPCR.

2.6. Measurement of immunomodulatory antibacterial activity

2.6.1. Bacteria culture

S. aureus (ATCC 12600; American Type Culture Collection, Manassas, VA, USA) was cultivated in trypticase soy broth (TSB) and -agar (TSA). A single colony was selected and cultivated overnight in 10 mL of TSB at 37 °C. Subsequently, the cells were diluted in fresh TSB and adjusted to a concentration of approximately 1×10^9 CFU/mL.

2.6.2. In vitro antibacterial tests

For antibacterial rate, 10^6 CFU of *S. aureus* was seeded on Ti and Ti-UV in standard 24-well polystyrene culture plate, and incubated aerobically at 37 °C for 1, 6, 18, 24 h. After incubation, the bacteria adhered to the samples were collected ultrasonically for 5 min in 5 mL fresh broth, diluted and plated onto TSA culture medium plate. Following incubation for 24 h, the CFU per plate was quantitated by plate count method. This experiment was repeated thrice.

2.6.3. Immunomodulatory antibacterial activity assay in co-culture systems

Three different co-culture systems were performed as follows: macrophages preferentially inoculated before *S. aureus* for 24 h (cell first coculture model), *S. aureus* preferentially inoculated before macrophages for 1 h (*S. aureus* first coculture model), and simultaneous coculture model. RAW264.7 cells were seeded at a density of 10^5 cells/well and cultured with antibiotic-free medium. 10^6 CFU of *S. aureus* was added and co-cultured with macrophages for 3 h for all groups (37 °C;

5% CO₂). Thereafter, all the samples were washed with PBS thrice to remove dead cells and non-adhered bacteria. To observe cell morphology and bactericidal effects of macrophages on different samples, the cell-bacteria on samples were washed, fixed, and dehydrated under the same treatments as described in Section 2.4 and analyzed by SEM observation.

Next, the macrophages were permeabilized and lysed with 0.1% Triton X-100 for 5 min to release phagocytosed *S. aureus*. Following that, the lysates were collected with PBS and performed 3 times of centrifugation and washed with PBS. Phagocytosed *S. aureus* was then stained for 15 min with Live/Dead® BacLight™ bacterial viability kit (L7012) following the manufacturer's instructions and photographed under an LSM700 confocal laser-scanning microscope (Carl Zeiss Ltd., Oberkochen, Germany) immediately. Each experiment was performed at least three times for each group.

To determine the bactericidal activity of macrophages on different sample surface, ROS generation was also detected using fluorescence staining. After co-culturing for 3 h, all samples were washed with PBS to remove dead cells and non-adhered *S. aureus*. The medium was then replaced with 1 mL antibiotic-free medium containing 5 µM CellROX® oxidative stress reagents (C10422, Thermo Fisher Life Technologies Ltd., Tokyo, Japan) and 4',6-diamidino-2-phenylindole (DAPI) at 37 °C for 15 min, and fixed in 4% paraformaldehyde for 15 min, then imaged using an LSM700 confocal laser-scanning microscope (Carl Zeiss Ltd., Oberkochen, Germany).

2.7. Osteogenic differentiation of rBMMSC in macrophage-conditioned medium

2.7.1. Growth and morphology of rBMMSC

After culturing for 3 and 24 h, rBMMSC in macrophage-conditioned medium of different groups were washed with PBS, fixed in 4% paraformaldehyde solution for 20 min and then permeabilized with 0.2% (v/v) Triton X-100 for 30 min. Following incubated with Blocking One reagent (Nacalai Tesque) for 30 min, rBMMSC were stained with phalloidin and 4',6-diamidino-2-phenylindole (DAPI) in darkness for 1 h. F-actin and cell nuclei were examined using a confocal laser-scanning microscope (LSM700; Carl Zeiss).

2.7.2. Osteogenesis and osteoclastogenesis-related gene expression of rBMMSC

To investigate whether RAW264.7 cells from different samples could regulate osteogenesis of rBMMSC, a macrophage-rBMMSC co-culture system was established using the conditioned medium (CM) method. RAW264.7 cells both with and without LPS stimulation were collected and mixed with MEM as above. The rBMMSC cells were seeded onto a 24-well plate at a density of 4×10^4 cells per well and incubated at 37 °C for 24 h. After incubation, the culture medium was removed and replaced by CM. Bone-related genes, alkaline phosphatase (ALP), bone morphogenetic protein 2 (BMP-2), runt-related transcription factor 2 (Runx2), and bone carboxyglutamate (gla) protein (Bglap), and osteoclastogenesis-related genes, OPG, RANKL, and MCSF, were analyzed by RT-qPCR after 3 and 7 d of culture.

2.7.3. Alkaline phosphatase (ALP) activity of rBMMSC

After incubation for 7 and 14 d, the cells were washed with PBS, lysed with 300 µL of 0.2% Triton X-100, and transferred to micro-centrifuge tubes. ALP activity was measured using the ALP pNPP Liquid Substrate and enzyme-linked immunosorbent assay (ELISA) Kit (Sigma-Aldrich, St Louis, MO, USA). The reaction was terminated by adding 50 µL of 3 N NaOH to the 200 µL reaction substrate, and *p*-nitrophenol production was determined at 405 nm with a 96-well microplate reader (SpectraMax® M5; Molecular Devices). DNA content was determined using the PicoGreen dsDNA Assay Kit (Thermo Fisher Scientific), and the amount of ALP was normalized against the amount of DNA in the respective cell lysates.

2.7.4. Mineralization of rBMMSC

To identify mineralization nodules, a Calcium E-Test Kit (Wako Pure Chemical Industrials) was used to quantify the amount of calcium on days 21 and 28 after rBMMSC growth in CM both with and without osteogenic supplements. Briefly, 1 mL of Calcium E-Test reagent and 2 mL of kit buffer were mixed. After which, the solutions were added to cells on different samples, and the absorbance (612 nm) of the reaction products was measured and calculated using a 96-well microplate reader (SpectraMax® M5; Molecular Devices).

2.8. In vivo evaluation of osteointegration

2.8.1. Surgical procedure

The animal procedures and experiments were carried out in accordance with the ethical principles of the National Institutes of Health guide for the care and use of Laboratory animals, and were approved by the Medical Ethics Committee of Osaka Dental University (Approval No. 20-02004). Briefly, 8-week-old male Sprague-Dawley rats, weighing 180–200 g each, were used in this study. After general anesthesia, the distal aspects of the femurs were carefully exposed via a 10-mm vertical skin incision at the knee joint. A 1.2-mm pilot hole was drilled into the distal femurs. Ti and Ti-UV screws were then randomly implanted in the bilateral femurs of the rats. The surgical sites were then carefully closed in layers. Eight weeks after surgery, rats were sacrificed by intraperitoneal injection of sodium pentobarbital, and the bilateral femurs containing implants were harvested.

2.8.2. Micro-CT evaluation

Micro-computed tomography (CT) system (Shimadzu, Tokyo, Japan) at 70 kV and 118 mA was applied to investigate the effects of the newly formed bone around the implants. The bone volume fraction (BV/TV), trabecular number (Tb.N), trabecular separation (Tb.Sp), and trabecular thickness (Tb.Th) within the regions of interest (ROI; 500 µm around the implant and 2 mm below the epiphyseal line) in the CT images were determined using Morphometric software (TRI/3D-BON; Ratoc System Engineering, Tokyo, Japan).

2.8.3. Histological evaluation

After Micro-CT scanning, the femoral specimens were collected, dehydrated, and stained with hematoxylin and eosin (H&E) to observe bone formation under a BZ-9000 digital cold illumination microscope (Keyence Co, Osaka, Japan).

2.9. Statistical analysis

All experiments were performed at least three times, and the data were expressed as mean ± standard deviation. Statistical significance was determined by performing one-way analysis of variance (ANOVA) followed by Bonferroni's *post hoc* test for three group comparison and Student-test for two group comparison. SPSS v. 20.0 (IBM Corp., Armonk, NY, USA) was used for statistical analysis, and *P* < 0.05 was considered significant.

3. Results

3.1. Surface characteristics

The surface morphology of Ti and Ti-UV samples was examined using SEM, and the results were illustrated in Fig. 1A. The Ti-UV discs showed no obvious differences compared to Ti. The XPS spectrum in Fig. 1B showed that the C1 peak was decreased on Ti-UV. Next, the water contact angles on the samples showed that the Ti samples were hydrophobic, exhibiting a contact angle of 64.9°. In contrast, Ti-UV discs were hydrophilic, with a significant decrease of the contact angle to 0° (Fig. 1C).

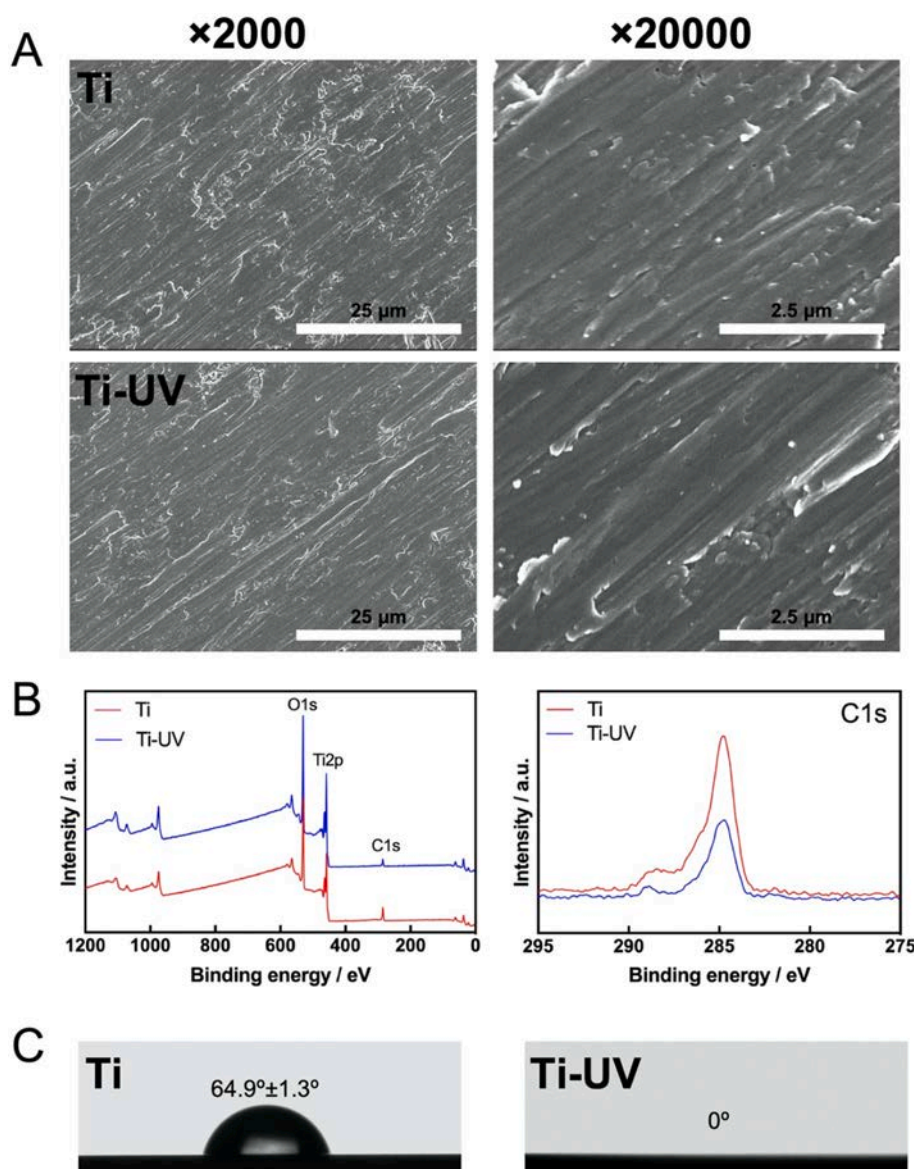


Fig. 1. Surface characteristics of Ti and Ti-UV. (A) SEM images of Ti and Ti-UV. (B) XPS analysis results of Ti and Ti-UV. (C) Contact angle of Ti and Ti-UV.

3.2. Effects of UV/ozone treatment of titanium on manipulating the immune response of macrophages

Growth and morphology of macrophages on all samples were showed by SEM (Fig. 2A). Macrophages grown on the Ti-UV surface showed a flatter and more elongated spindle shape, with a larger attachment area than those on Ti surface. In addition, based on the cell viability assay, Ti-UV had higher levels of cell adhesion and proliferation, indicating that UV/ozone treatment enhanced the biocompatibility of titanium. (Fig. 2B).

To evaluate the immunoregulatory effects of UV/ozone treatment on macrophage polarization and inflammatory response, the intensity of M1-related surface marker, CD11c, was measured by flow cytometry (Fig. 2C). The mean fluorescence intensity of CD11c was decreased on Ti-UV, suggesting that the UV/ozone treatment might have inhibited the pro-inflammatory responses of titanium.

Further, M1- and M2-related gene expression was analyzed by RT-qPCR after macrophages incubation for 3 and 6 d. Expression of pro-inflammatory genes, including TNF- α and IL-6, were significantly downregulated on Ti-UV, while that of anti-inflammatory genes, including IL-10 and Arg1, were significantly upregulated on Ti-UV

(Fig. 2D). These results demonstrate that the level of pro-inflammatory responses of macrophages was inhibited by UV/ozone treatment.

Additionally, mRNA expression of osteogenic, fibrogenic, and angiogenic-related genes were also examined, which play a vital role in forming new bone formation. Results showed that macrophages cultivated on Ti-UV had greater gene expression than Ti (Fig. 2E).

3.3. Effects of UV/ozone treatment of titanium on the immune response of macrophages in LPS activated inflammatory condition

LPS was used to activate the acute inflammatory response of macrophages on different samples. The cell morphology and viability of macrophages are shown in Fig. 3A, B. The SEM images display different affinities of macrophages to Ti and Ti-UV surface. In the situation with LPS stimulation, macrophages lysis was obviously observed on Ti surface, while no macrophage lysis occurred on Ti-UV surface. Furthermore, macrophages grown on Ti-UV surface had star-like shapes with apparent synapse and exocytotic vesicles. Higher cell viability was also detected on the Ti-UV (Fig. 3B).

To measure mitochondrial oxidative stress, mitochondrial

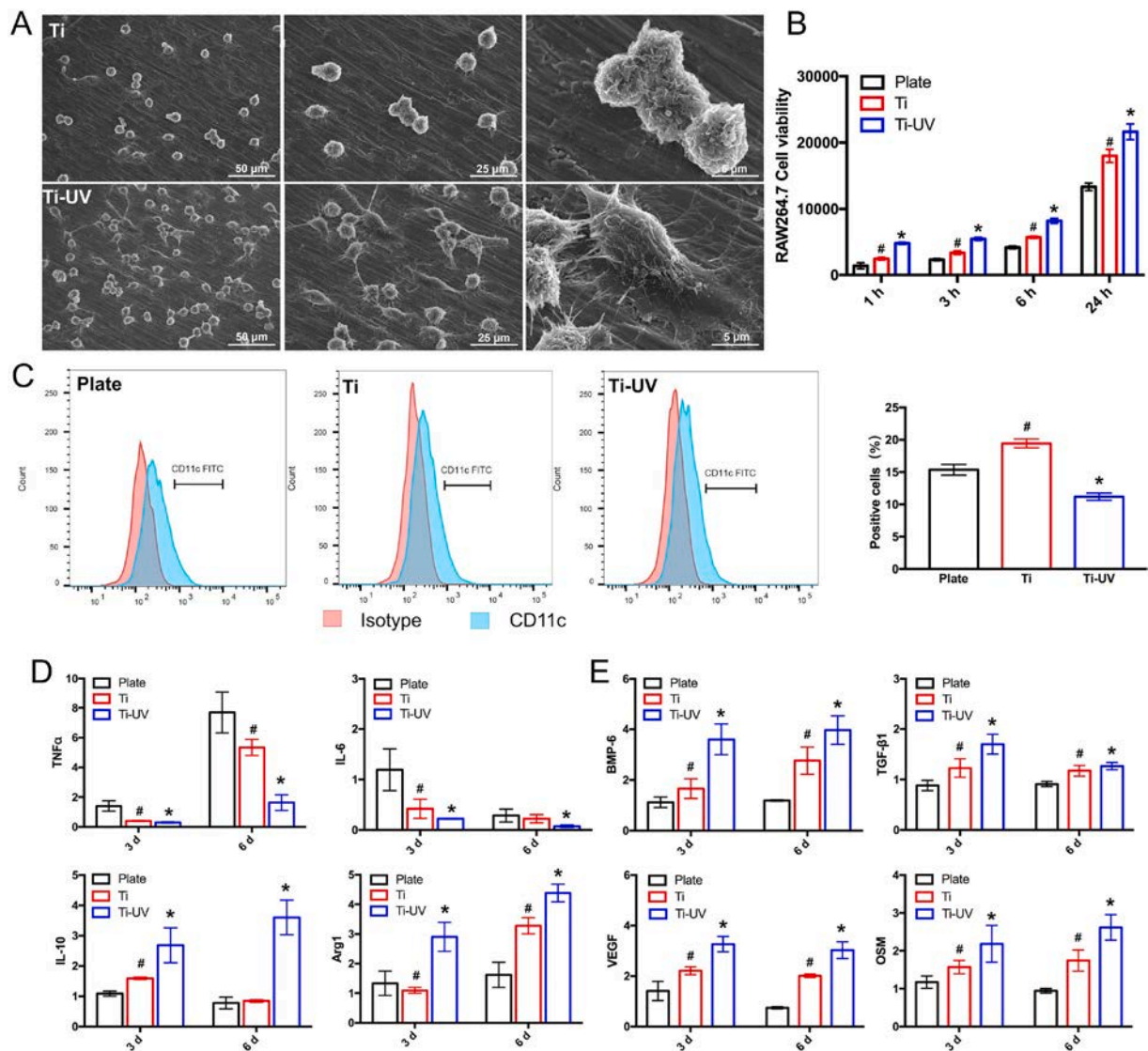


Fig. 2. Effects of UV/ozone irradiation on the ability of titanium to manipulate macrophage immune response. (A) Cell growth and morphology of RAW264.7 on samples, determined by SEM. (B) Cell viability of RAW264.7. (C) Flow cytometry analysis of the M1-related marker CD11c of RAW264.7. (D) Real-time polymerase chain reaction (RT-qPCR) of the gene expression of M1-related TNF- α , IL-6, and M2-related IL-10, Arg1. (E) RT-qPCR analysis of the osteogenic-related gene expression of BMP-6, TGF- β , VEGF, and OSM. (# represents $p < 0.05$ when Ti is compared with Plate; * represents $p < 0.05$ when Ti-UV is compared with Ti).

membrane potential changes of macrophages were monitored via JC-1 staining. Fluorescence microscopy showed that, in the Ti-UV group, RAW 264.7 cells had strong J-aggregation (red) and weak JC-1 monomer (green) levels. In contrast, in the plate and Ti groups, the cells showed higher JC-1 monomer (green) levels with concomitantly decreased J-aggregation (red) due to low $\Delta\Psi_m$, indicating the inhibition of LPS-induced polarization of $\Delta\Psi_m$ and mitochondrial oxidative stress on Ti-UV (Fig. 3C). Consistently, macrophages on plate and Ti displayed significantly higher levels of intracellular ROS than Ti-UV (Fig. 3D), suggesting that the UV/ozone treatment of titanium showed great biocompatibility in macrophages.

The expression of M1- and M2-related genes of LPS-activated macrophages on different substrates was further measured by RT-qPCR (Fig. 3E). Results revealed that LPS increased expression of all M1-related genes (TNF- α and IL-6), while Ti-UV slightly downregulated M1-related gene expression. Correspondingly, the levels of M2-related genes IL-10 and Arg-1 were significantly upregulated on Ti-UV, implying that the UV/ozone treatment of titanium can inhibit pro-inflammatory macrophages and promote expression of M2-related genes, even in an inflammatory microenvironment.

Furthermore, the expression of osteogenic, fibrogenic, and angiogenic-related gene expression was upregulated on Ti-UV (Fig. 3F). Taken together, our results indicate that Ti-UV possessed effective osteoimmunomodulatory functions even in LPS activated inflammatory condition.

3.4. Antibacterial activity of UV/ozone treatment of titanium on manipulating the immune response of macrophages against *S. aureus*

3.4.1. Antibacterial activity of UV/ozone treatment of titanium

Before cell-bacteria cocultured, the antibacterial abilities of Ti-UV against *S. aureus* were tested and the results were showed in Fig. S1. Ti-UV exhibited superior antibacterial abilities against *S. aureus*, and showed higher antibacterial activity with increased culture time.

3.4.2. Immune response of macrophages against *S. aureus* with macrophage first coculture model

First, macrophages were cultured for 24 h and then cocultured with *S. aureus* for 3 h on Ti and Ti-UV surface. The SEM results (Fig. 4B) showed that *S. aureus* aggregation was observed on the cell surface but

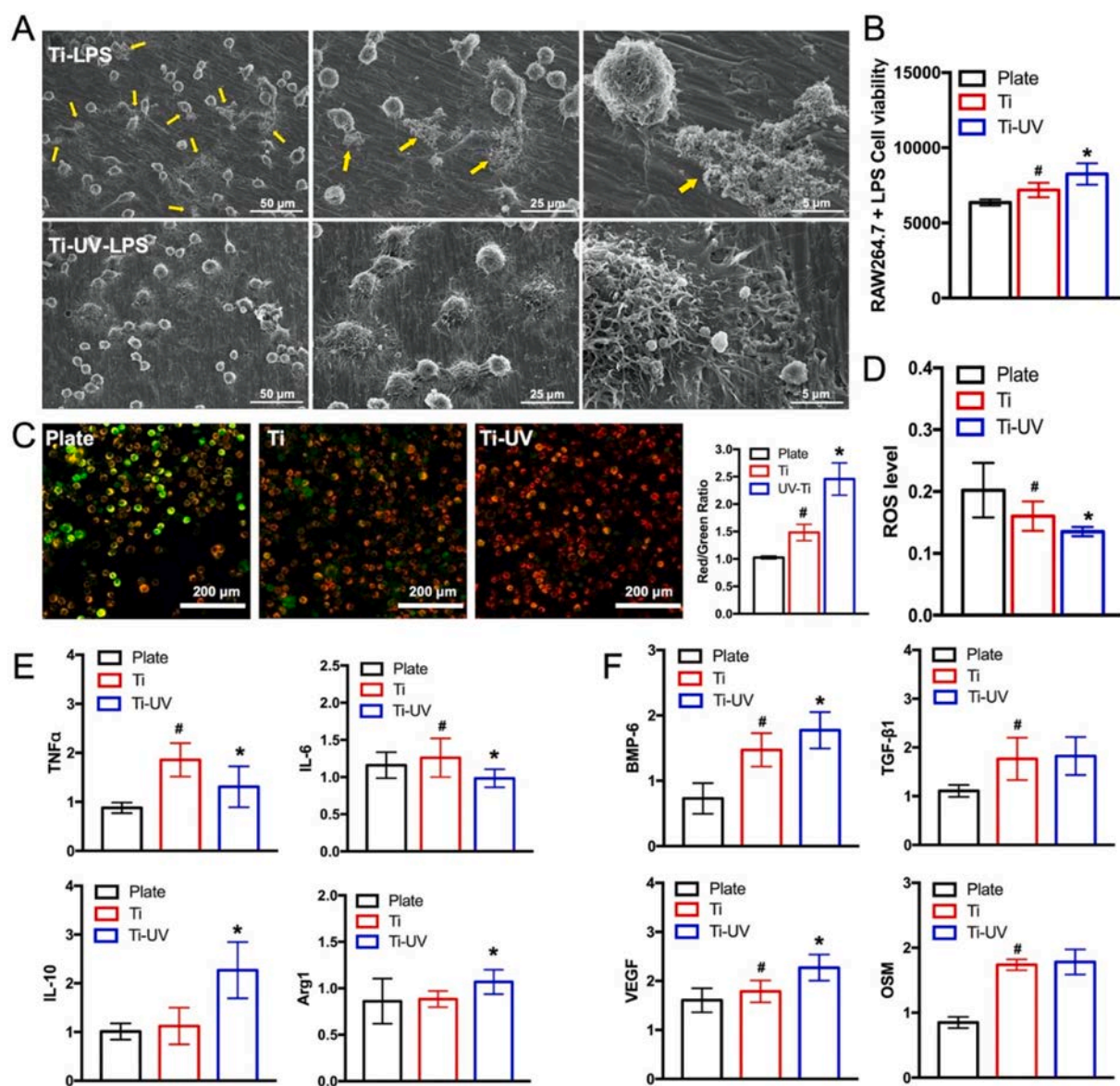


Fig. 3. Effects of UV/ozone irradiation on the ability of titanium to manipulate macrophage immune response in LPS-activated inflammatory condition. (A) Cell growth and morphology of LPS-activated RAW264.7 on samples, determined by SEM. (Yellow arrows represent lysed macrophages.) (B) Cell viability of LPS-activated RAW264.7. (C) Mitochondrial membrane potential changes of LPS-activated macrophages accessed via JC-1 staining and detected by fluorescence microscopy. Red, healthy cells; Green, apoptotic or unhealthy cells. (D) Intracellular Reactive Oxygen Species (ROS) Level of LPS-activated RAW264.7. (E) RT-qPCR of the gene expression of M1-related TNF- α , IL-6, and M2-related IL-10, Arg1. (F) RT-qPCR analysis of the osteogenic-related gene expression of BMP-6, TGF- β , VEGF and OSM. (# represent $p < 0.05$ when Ti compared with Plate; * represent $p < 0.05$ when Ti-UV compared with Ti). (For interpretation of the references to colour in this figure legend, the reader is referred to the web version of this article.)

not on the sample surface. Higher growth of macrophages that exhibited longer spindle-shapes and extended cell pseudopodia were observed in the Ti-UV groups, while cells on the Ti surface exhibited round shape and more bacteria on the surface of the cells.

The phagocytosis of macrophages on *S. aureus* were observed by fluorescence staining images. As Fig. 4C reveals that macrophages on Ti-UV surface phagocytosed more *S. aureus* than Ti group. Next, ROS generation was also detected using fluorescence staining (Fig. 4D) to determine the bactericidal activity of macrophages on different sample surface. Macrophages on both Ti and Ti-UV surfaces produced high amounts of ROS, and higher level of ROS generation was observed in Ti-UV group. These results suggest that the immune response of macrophages was significantly enhanced by UV/ozone treatment of titanium with great viability and phagocytic activity.

3.4.3. Immune response of macrophages against *S. aureus* with *S. aureus* first coculture model

We, next, preferentially inoculated *S. aureus* for 1 h and then cocultured with macrophages for 3 h on different samples. With the *S. aureus* first coculture model, macrophages displayed significantly flatter morphological change that tended to spread better interactions on surface. Moreover, fewer macrophages growth and more cell lysis were observed on the Ti surface, and engulfed *S. aureus* were observed inside the lysed macrophages. More macrophages growth and extra-cellular vesicles around cells were observed on Ti-UV surface. (Fig. 5B).

Unlike the cell first coculture model, more *S. aureus* cells adhered to sample surfaces, and the adhered and engulfed *S. aureus* were collected and observed by fluorescence staining. Fewer *S. aureus* was observed on Ti-UV, which suggests a higher antibacterial activity of Ti-UV (Fig. 5C). ROS fluorescence staining images showed that macrophages of Ti groups

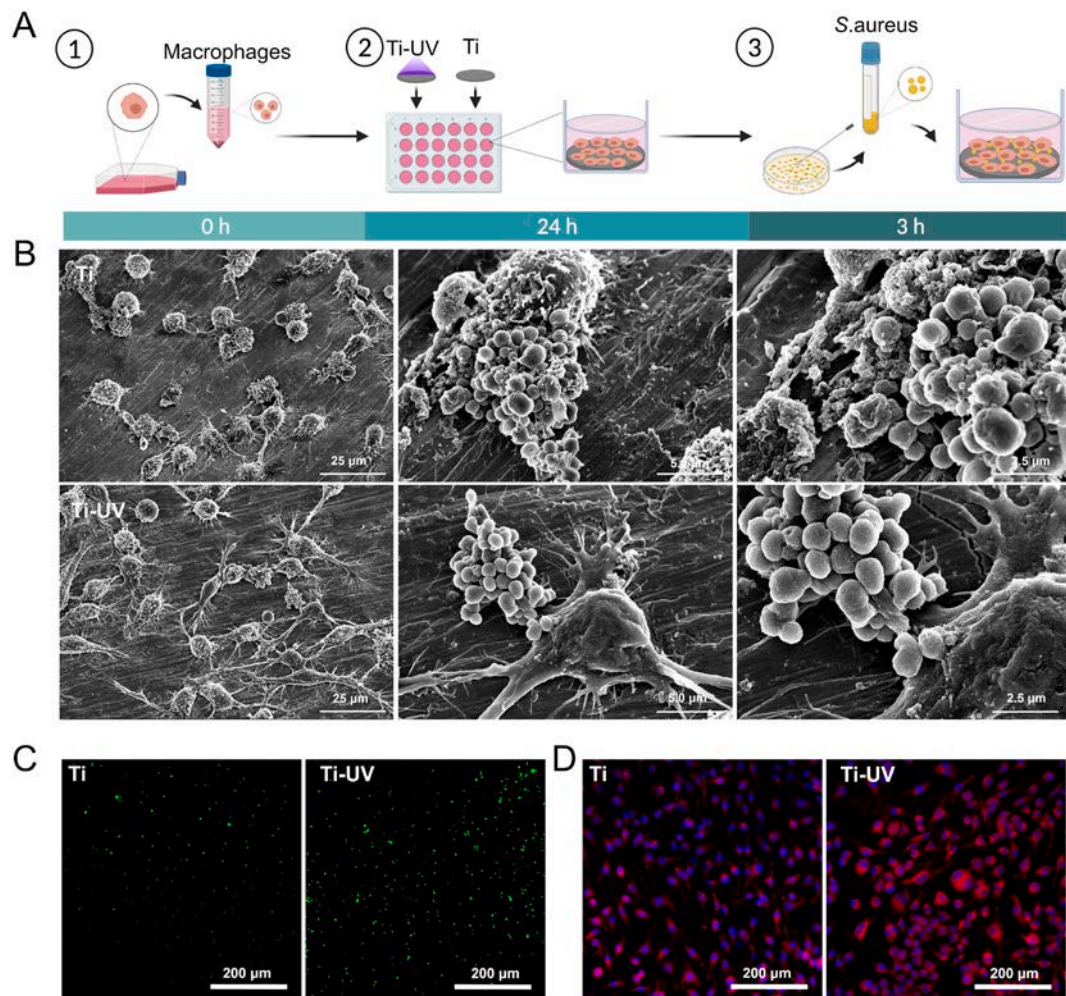


Fig. 4. Effect of UV/ozone irradiated titanium on manipulating macrophage immune response against *S. aureus*, with macrophage first coculture model. (A) Schematic diagram of the cell and bacteria co-culture process. (B) Cell morphology, growth and bactericidal effects of macrophages on different samples, determined by SEM. (C) Phagocytosis of sample-conditioned macrophages against *S. aureus* detected by fluorescence microscopy. (D) ROS generation of macrophages on samples, determined by fluorescence microscopy.

generated less ROS, while those of Ti-UV groups generated more, indicating the great phagocytic activity of macrophages on Ti-UV surface (Fig. 5D).

3.4.4. Immune response of macrophages against *S. aureus* with simultaneous coculture model

To assess the race between macrophages and *S. aureus* for occupying the sample surfaces, macrophages and *S. aureus* were incubated simultaneously for 3 h. Macrophages on Ti and Ti-UV surface displayed both round and flat shapes, with those on the Ti-UV surface being flatter (Fig. 6B). Elongated pseudopodia on the Ti surface, and damaged *S. aureus* trapped by macrophage on Ti-UV were also observed, which related the process of macrophages to phagocytosis that kills bacteria.

Fluorescence staining images (Fig. 6C, D) showed lower number of *S. aureus* and higher level of ROS generation on Ti-UV surface, suggesting that Ti-UV could effectively suppress bacteria adhesion and modulate the macrophages with enhanced immune response against bacteria.

3.5. Osteogenic differentiation of rBMSC in macrophage-conditioned medium

Growth and morphology of rBMSC in macrophage-conditioned medium from different samples were investigated with fluorescence

staining. Fig. S2 indicates that rBMSC in Ti-UV macrophage-conditioned medium attached and spread better.

Expression of osteogenic genes (Runx2, BMP-2, Bglap) and osteoclastogenesis-related genes (M-SCF, RANKL, OPG) of the Ti-UV groups were upregulated compared to those of other groups at 3 and 7 d (Fig. 7B, C). Highest ALP activity and mineralization level were also observed in Ti-UV groups. (Fig. 7D).

In the proinflammatory condition (with LPS), the osteogenic differentiation of rBMSC in all groups was inhibited, including osteogenic gene expression, ALP activity, and mineralization levels of rBMSC. Nevertheless, as compared with Plate and Ti, the osteogenic differentiation of cells on the Ti-UV surface was enhanced (Fig. 8B, D). Furthermore, the osteoclastogenesis-enhancing genes, M-SCF and RANKL, were remarkably downregulated, while the osteoclastogenesis-inhibiting gene OPG was upregulated in the Ti-UV group (Fig. 8C). These results suggest the superior ability of the UV/ozone treatment of titanium to create a favorable osteoimmune environment and promote osteointegration.

3.6. In vivo evaluation of osteointegration

The histological sections (Fig. 9A) showed that Ti implants still exhibited fibrous connective tissue from the bone-implant interface, whereas the Ti-UV implants were almost entirely surrounded with new

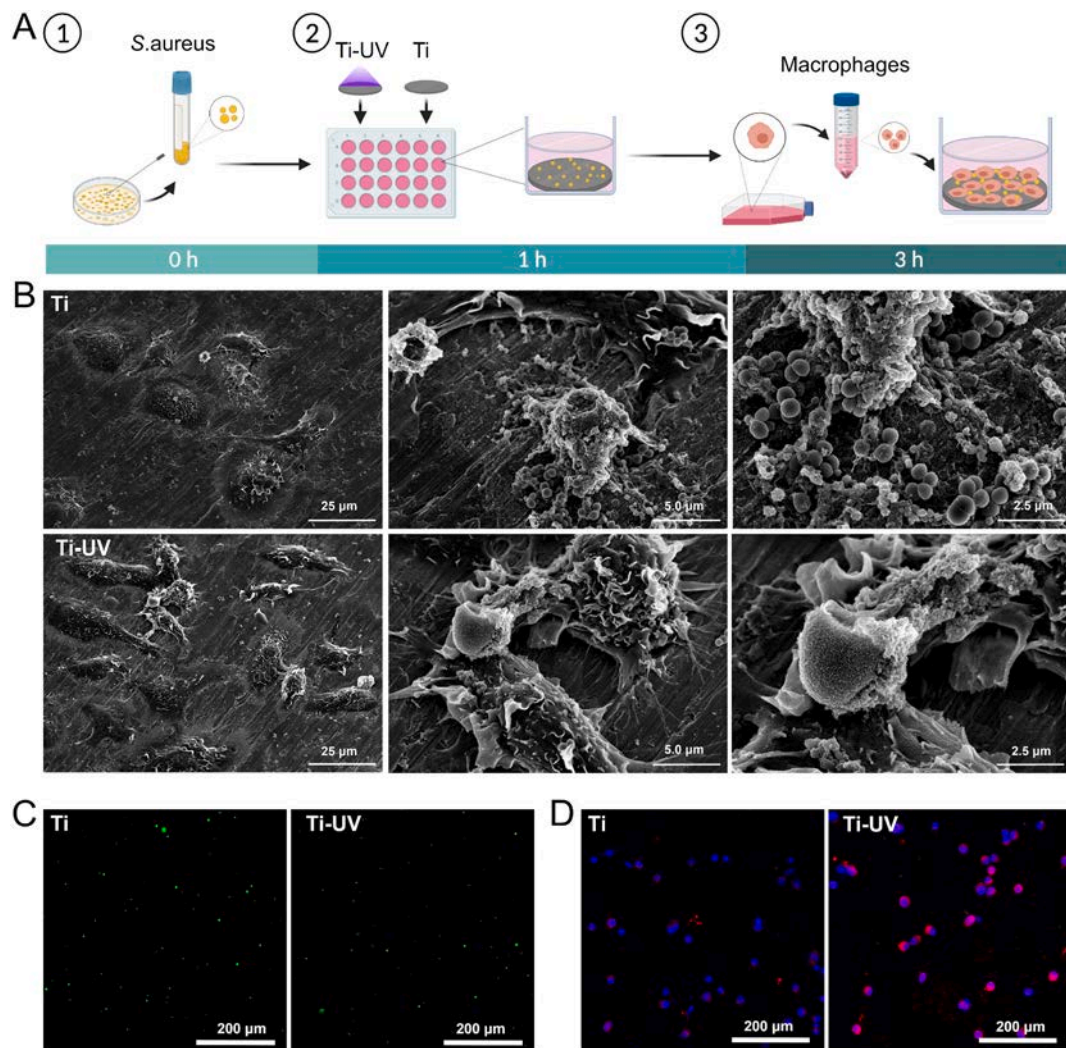


Fig. 5. Effect of UV/ozone irradiated titanium on manipulating macrophage immune response against *S. aureus*, with *S. aureus* first coculture model. (A) Schematic diagram of the cell and bacteria co-culture process. (B) Cell morphology, growth, and bactericidal effects of macrophages on different samples, determined by SEM. (C) Phagocytosis of sample-conditioned macrophages against *S. aureus*, detected by fluorescence microscopy. (D) ROS generation of macrophages on samples determined by fluorescence microscopy.

bone. The bone area ratio (BA) and bone implant contact (BIC) were unregulated on Ti-UV (Fig. 9B). The reconstructed three-dimensional micro-CT images of rat femoral transverse slices showed that thin new bone layers formed around the implants after 8 weeks on Ti, while Ti-UV group exhibited larger bone volume and higher trabecular numbers surrounding the implants (Fig. 9C). Further, the BV/TV, Tb.N, and Tb.Th were significantly higher in the Ti-UV group, suggesting better quality and quantity of bone formation surrounding the Ti-UV implants (Fig. 9D).

4. Discussion

Insufficient bone biomaterial-associated infections and osseointegration are the most common challenges in orthopedic and dental surgeries [42–44]. Efforts have been made to produce anti-infectious modification of titanium, mostly by coating antibacterial nanoparticles, such as Au [45,46], Ag [47,48], Zn [49], and Cu [35], onto titanium surface. However, these nanoparticles can induce toxic effects, including excessive ROS induction, mitochondrial damage, DNA damage, cell death, and negatively impact different tissues and organs, which limit their clinical application [50–52]. Different from these nanoparticles, studies demonstrated that various types of UV instruments could

markedly enhance both antibacterial properties and osteoconductive capacity of different biomaterials [38–40]. With the rapid development of UV technology in modification of biomaterials, there are many fields where conventional UV treatment methods are insufficient, and several new UV irradiation methods combined with low-dose ozone have been developed. UV/ozone irradiation is believed to have greater clinical potential both in preventing biomaterials-associated infections and in achieving favorable bone formation [41].

Most recently, innate immune system is expected to meet the needs for preventing and curing biomaterials-associated infections and bone fracture healing [53,54]. Among various immune cells, macrophages are the first cells to arrive at the fracture site to defense bacterial invasion through production of oxidative bursts, proinflammation cytokines, and bacterial peptides [55,56]. Macrophages are capable of ingesting and destroying invading pathogens, and can promote antigen presentation on their surface, eliciting adaptive immune responses [57]. UV/ozone surface modification could induce changes to surface chemistry and produce a large number of bone cell proliferation onto the surface of biomaterials [58]. However, the mechanisms on the immunomodulatory antibacterial activity and the microenvironment of immune cell-osteoblast crosstalk of UV/ozone irradiation are little known. Herein, we first evaluated the macrophage-mediated immunomodulatory

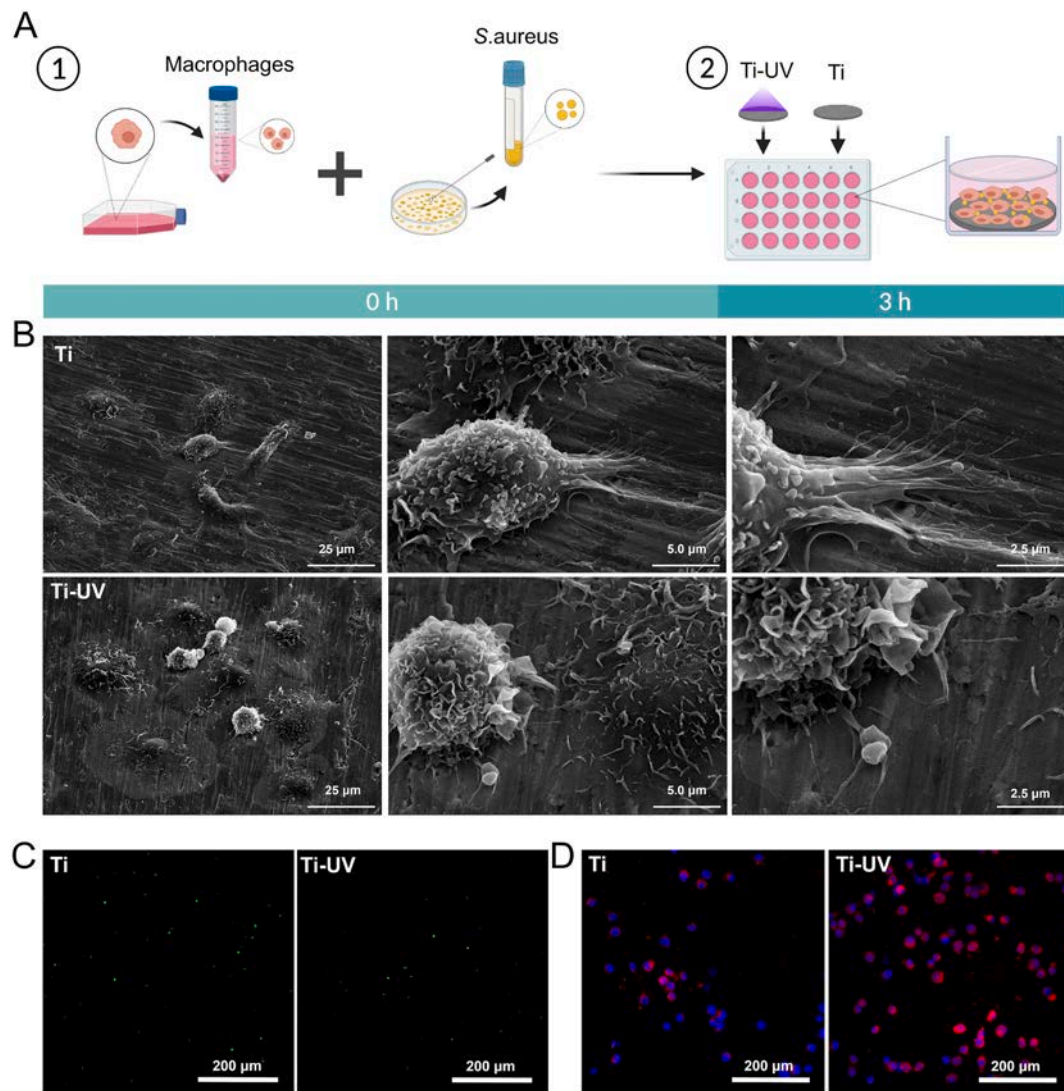


Fig. 6. Effect of UV/ozone irradiated titanium on manipulating macrophage immune response against *S. aureus* with simultaneous coculture model. (A) Schematic diagram of the cell and bacteria co-culture process. (B) Cell morphology, growth and bactericidal effects of macrophages on different samples determined by SEM. (C) Phagocytosis of sample-conditioned macrophages against *S. aureus*, detected by fluorescence microscopy. (D) ROS generation of macrophages on samples determined by fluorescence microscopy.

antibacterial activity with development of three different cell and bacteria co-culture models on different sample surfaces and macrophage and MSC co-culture systems to understand the osteoimmunomodulation of UV/ozone irradiated titanium. *In vitro* and *in vivo* studies proved that UV/ozone irradiation could significantly manipulate the immune response of macrophages against *S. aureus* with excellent bactericidal activity and also generate a favorable osteoimmune microenvironment on titanium.

In the present study, we established three different co-cultured models to better mimic colonization on biomaterials, including a cell first model, a bacterial first model, and a simultaneous coculture model [59,60]. We found that under three different co-cultured models, the behavior of macrophages is completely different. In the cell first coculture model, macrophages revealed excellent attachment and proliferation on the surface of implant before *S. aureus* was added. Therefore, *S. aureus* was quickly internalized by the macrophages and engulfed into the phagosome. Macrophages then produced a large amount of ROS that contributed to bactericidal activity. As shown in Fig. 4, more bacteria phagocytosed and higher ROS generation were assayed on the Ti-UV surface, which may be attributed to enhanced biological function of macrophages on Ti-UV surface. Compared to the cell first coculture

model, the *S. aureus* first coculture model (Fig. 5) and simultaneous coculture model (Fig. 6) showed less macrophages adhered, but more bacteria adhesion on sample surface. Interestingly, little macrophages on the Ti surface can produce ROS, while obviously almost all of the macrophages on the Ti-UV surface can produce ROS (Figs. 5D, 6D). It might be attributed to that macrophages, as latecomers, is difficult to survive and proliferate when bacteria occupy a first and dominant position, thereby could not immediately phagocytose and kill bacteria. These results suggested that UV/ozone irradiation of titanium significantly enhanced biological functions of macrophages and contributed to the modulation of immune response against bacterial infections. Our study might provide valuable insights and strategies for therapeutic interventions that investigate the competitive race between bacteria and host immune cells to attach to the surface of the biomaterial.

In this study, the dynamic transformation of macrophage phenotypic plasticity and the inflammation response in both physiological and pathological conditions were evaluated. Fig. 2C illustrated that the proportion of M1 phenotype of macrophages was lower in the Ti-UV group. Furthermore, higher M2-related gene expression (IL-10 and Arg-1) were detected in the Ti-UV group (Fig. 2D). Thus, UV/ozone irradiation can apparently inhibit macrophage polarization to M1

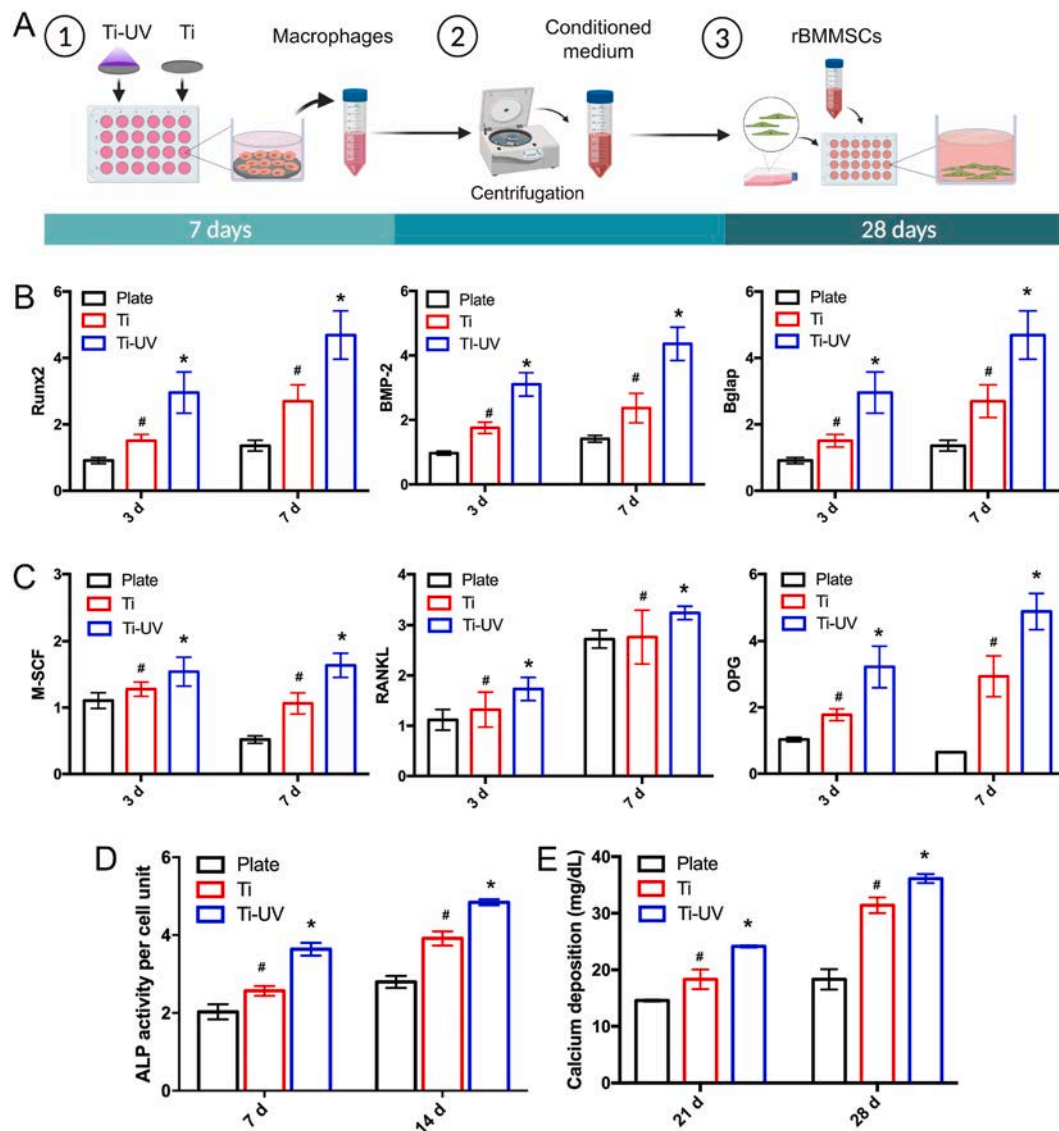


Fig. 7. Osteogenic differentiation of rBMMSCs in macrophage-conditioned medium. (A) Schematic diagram of the cell co-culture processing method. (B) RT-qPCR analysis of the osteogenic-related gene expression of Runx2, BMP-2 and Bglap. (C) RT-qPCR analysis of the osteoclastogenesis-related gene expression of MSC-F, RANKL, and OPG. (D) ALP activity levels on days 7 and 14. (E) Mineralization level on days 21 and 28. (# represent $p < 0.05$ when Ti compared with Plate; * represent $p < 0.05$ when Ti-UV compared with Ti).

phenotype and enhance the osteogenesis in physiological conditions. In LPS-stimulated conditions, macrophages were polarized towards a pro-inflammatory M1 phenotype, and the expression of M1-related genes was significantly upregulated (TNF- α and IL-6) in all groups, with Ti-UV showing the lowest expression levels (Fig. 3E). The general paradigm of macrophages polarization suggests that M1 macrophages predominate in early stages of the healing and contribute to the clearance of the debris from the fracture site, while M2 macrophages predominated in later stages for secreting growth factors that support matrix mineralization and bone formation [61]. TNF- α and IL-6 are pleiotropic proteins that can regulate the cell death of inflammatory tissues, modify vascular endothelial permeability, and induce production of acute-phase proteins [62]. Together with other pro-inflammatory cytokines, TNF- α triggers transient activation of TNF- α and JAK-STAT signaling pathways, and contributes to the high expression of transcription factors such as NF- κ B [63,64]. Studies have demonstrated that LPS induces excessive ROS production and reactive nitrogen species (RNS) in macrophages, leading to upregulation of proinflammatory mediators, impaired immune response, oxidative DNA damage, and mutation frequency [65,66].

Further, it has been found that excessive ROS production can create a positive feedback loop of autocrine TNF- α -mediated expression by releasing oxidized peroxiredoxin-2 (PRDX2) [67,68] and promote TNF- α -induced cell death [69,70]. Here, the mitochondrial membrane potential changes and intracellular ROS levels (Fig. 3C, D) were significantly downregulated on Ti-UV in LPS-stimulated conditions, and might have been responsible for the observed inhibition of pro-inflammation gene expressions. Interestingly, in the presence of bacteria, the macrophages on the Ti-UV surface produced more ROS. From this, we speculated that the performance of macrophages in different biological microenvironments is different, and the effects of ROS on cells are also different. In a pathogen-free environment, Ti-UV surface inhibits the production of excess ROS so that macrophages gain better proliferation ability. However, in the presence of pathogens, UV/ozone irradiated titanium assists macrophages to not only maintain their own survival, but also exert bactericidal function. Taken together, the findings suggest that UV/ozone irradiation of titanium changed the cell intracellular microenvironment and the subsequent signaling cascade and participated in regulating the inflammation response, thereby enhancing tissue

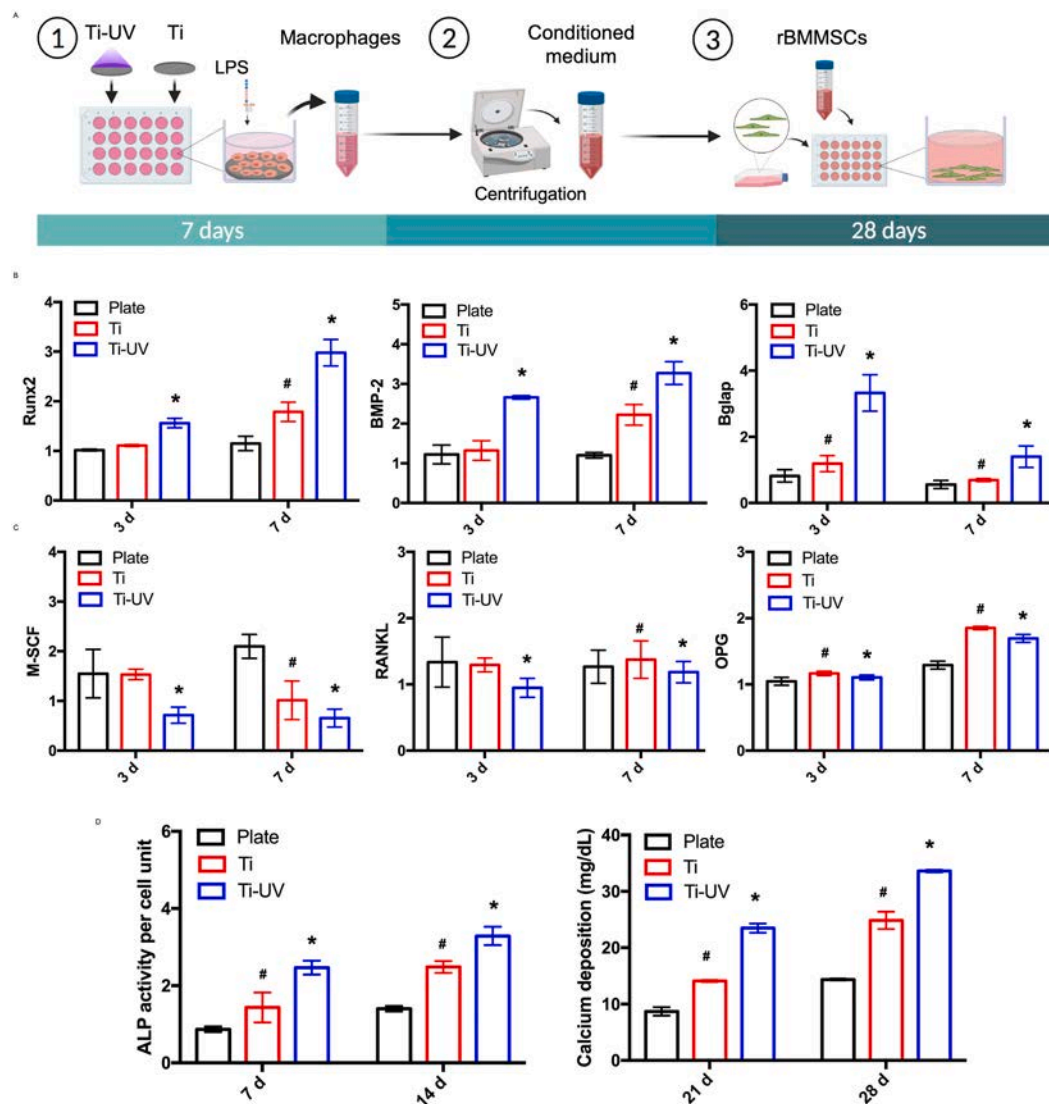


Fig. 8. Osteogenic differentiation of rBMSCs in LPS-activated macrophage-conditioned medium. (A) Schematic diagram of the cell co-culture processing method. (B) RT-qPCR analysis of the osteogenic-related gene expression of Runx2, BMP-2 and Bglap. (C) RT-qPCR analysis of the osteoclastogenesis-related gene expression of M-CSF, RANKL, and OPG. (D) ALP activity levels on days 7 and 14. (E) Mineralization level on days 21 and 28. (# represent $p < 0.05$ when Ti compared with Plate; * represent $p < 0.05$ when Ti-UV compared with Ti).

restoration outcomes.

Next, the effects of UV/ozone irradiated titanium on the osteogenic gene expression in macrophages both with and without LPS (Figs. 2E, 3F) were analyzed, including those of BMP-6, TGF β 1, VEGF, and OSM, which participate in osteogenesis, fibrosis, and angiogenesis. With elevated expressions of BMP-6 and OSM from macrophages, the BMP-6 and OSM pathway can be activated, which mainly contribute to enhanced osteogenesis [71,72]. Guihard et al. [73] demonstrated that LPS induced OSM production from monocytes/macrophages via COX-2 and PGE2, and that OSM signaling via gp130 on MSC was mainly responsible for the enhanced osteogenesis. Macrophages on the Ti-UV surface showed greater expression of osteogenic factors compared to plate and Ti, indicating that the UV/ozone irradiated titanium may generate an osteogenic microenvironment for better bone formation.

Bone biomaterials associated-bone remodeling is predominantly mediated by the immune system, and continuously undergoes coupled resorption and formation with osteoclasts and osteoblasts, respectively [74]. Osteogenic differentiation and osteoclastogenesis of rBMSC were examined via the conditioned medium method. With the LPS-added CM, the osteogenic inhibitory effects were mostly due to cytokine production

by macrophages, such as TNF- α and IL-6, since macrophages are the main targets of LPS [75,76] and are mostly responsible for the pro-inflammatory response but not in rBMSC. Results (Fig. 7B, D) showed that rBMSC cultured in CM of Ti-UV showed a tendency of advanced osteogenic differentiation, as indicated by an enhanced ALP activity, improved ECM mineralization, and upregulated osteogenic genes (ALP, BMP-2, Runx2, and Bglap), indicating that the biological composition produced by macrophages on Ti-UV might have remarkably enhanced osteogenic effects. Meanwhile, osteoclastogenesis of rBMSC was also measured since M-CSF, RANKL, and osteoprotegerin (OPG) are the most potent stimuli of osteoclastogenesis [77–79]. We observed that in the physiological microenvironment (Fig. 7C), M-CSF, RANKL, and OPG were all significantly increased, suggesting enhanced osteoclastogenesis and osteogenic activities, and further indicating that UV/ozone irradiation might have induced an active bone reconstruction process. However, in LPS-stimulated conditions (Fig. 8C), M-CSF and RANKL were significantly decreased on Ti-UV compared to that on Plate and Ti, suggesting that UV/ozone irradiation could suppress osteoclastogenesis activity in inflammation conditions. Studies have revealed that the pro-inflammation effect of immune cells could inhibit osteogenesis,

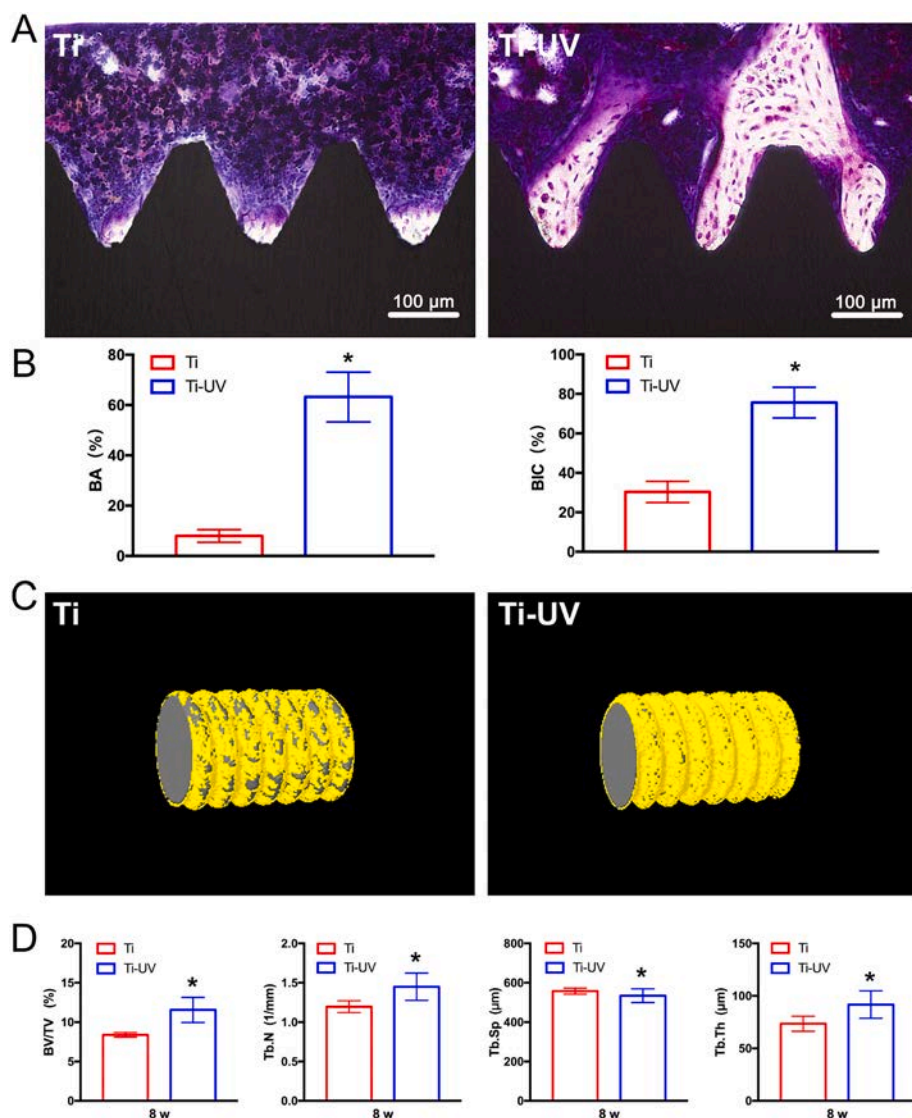


Fig. 9. *In vivo* evaluation of osteointegration in the SD rat femoral model. (A) Villanueva staining of bone tissue around implants. (B) Bone area ratio (BA) and bone-implant contact (BIC). (C) Micro-CT 3D reconstructions of the implants and surrounding bone. Gray represents the implant. Yellow represents the surrounding bone. (D) Bone volume fraction (BV/TV); trabecular number (Tb.N); trabecular separation (Tb.Sp); trabecular thickness (Tb.Th). (# represent $p < 0.05$ when Ti compared with Plate; * represent $p < 0.05$ when Ti-UV compared with Ti). (For interpretation of the references to colour in this figure legend, the reader is referred to the web version of this article.)

while anti-inflammation may have the opposite effects [80]. However, some recent studies have also confirmed the dual role of TNF- α in bone remodeling, such that the low-dose stimulus recruit osteoblasts, while the high-dose stimulus inhibits and transforms bone formation to resorption [81–83]. IL-6 is a main mediator of osteoclastogenesis, which can induce RANKL and participate in osteoclastogenic differentiation induced by TNF- α and IL-1 [84]. In this study, UV/ozone treatment of titanium downregulated pro-inflammation gene expression levels (TNF- α , IL-6) and upregulated anti-inflammation gene expression (IL-10, Arg-1) in macrophages, resulting in a lower osteoclastogenesis in rBMMSC, further indicating the great potential of Ti-UV in bone remodeling. Therefore, our studies proved that UV/ozone irradiation is valuable to enhance favorable osteoimmunomodulatory properties of titanium.

We next investigated the *in vivo* osteointegration of titanium implants. Consistent with the *in vitro* results, both histological evaluation (Fig. 9A, B) and micro-CT (Fig. 9C, D) revealed more new bone generation and higher bone-implant contact around the Ti-UV implants, indicating enhanced osseointegration capacity and reduced inflammation of UV/ozone irradiated titanium.

Numbers of studies proved that surface wettability and charge of biomaterials influence protein adhesion, cell growth, shape, and proliferation. Generally, most of the conditional ultraviolet surface modification irradiation devices emitting light at short wavelengths of 184.9

nm and 253.7 nm as the main wavelength are used. The shorter the wavelength, the larger the amount of energy of UV irradiation can greatly improve surface modification with higher molecular binding energy. At the same time, active oxygen (O) separated from ozone generated by UV irradiation chemically combines with organic pollutants, decomposes and reacts with volatile substances such as carbon dioxide and water, which remove them from the surface of the biomaterial. Herein, we employed a new type of UV irradiation device with the shortest wavelength of 172 nm combined with low-dose of ozone. As the results of Fig. 1, the superhydrophilicity and removal of oxygen-containing hydrocarbons with more Ti^{4+} by UV/ozone irradiation might promote adherence of biological components to the surface, thereby modulating the local microenvironment and cell responses. The Fig. 10 showed how UV/ozone irradiated titanium modulated the immune response for antibacterial activity and bone regeneration. Much still remains unknown about the underlying mechanisms linking these changes in surface characteristics to immune cellular behaviors, but our study elucidated this cellular cross-talk may hold great promise to provide tools for optimized balance of bone remodeling and accelerated osteointegration of bone biomaterials.

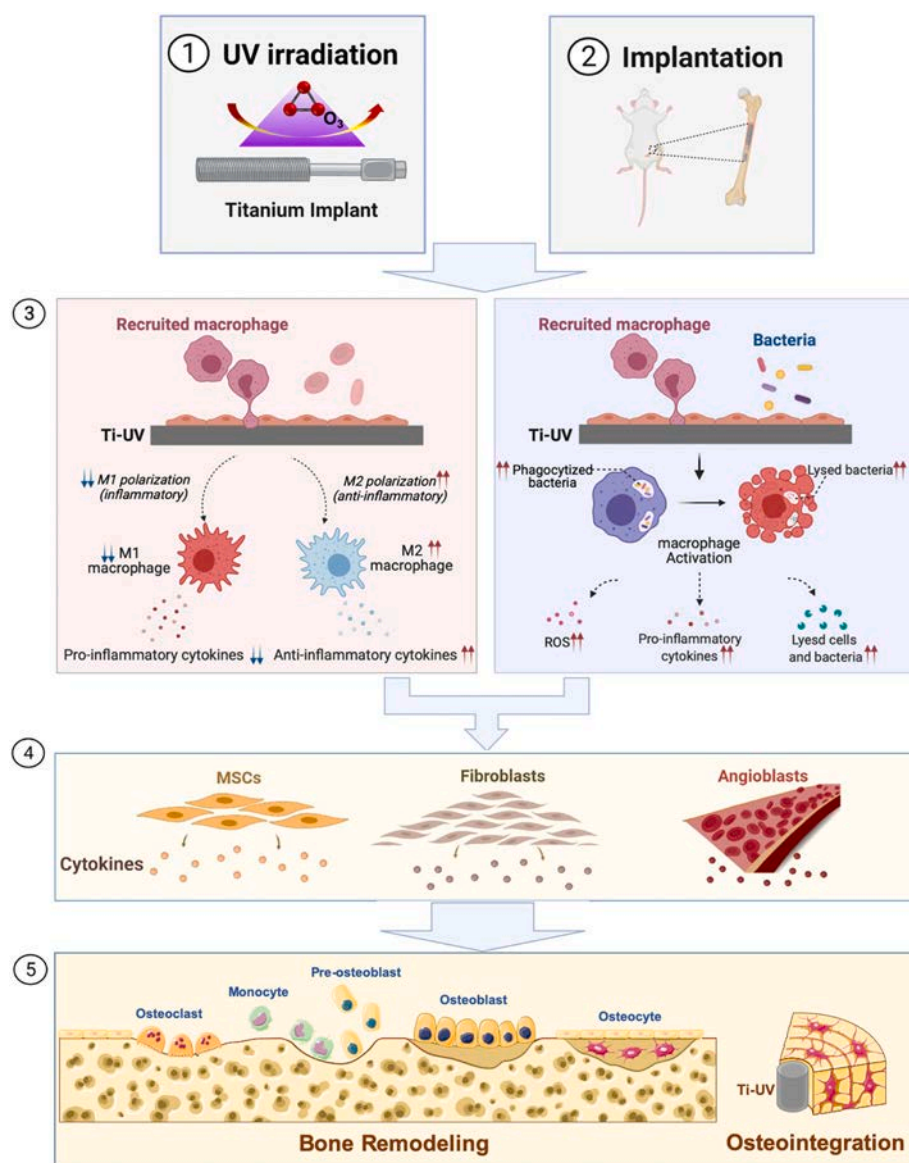


Fig. 10. The schematic showed how UV/ozone irradiated titanium modulated the immune response for antibacterial activity and bone regeneration. Following bone implantation, UV/ozone irradiated titanium biomaterials recruited macrophages, inhibited macrophage polarization to the M1 phenotype, and promoted polarization to the M2 phenotype. In the presence of bacterial invasion, the phagocytosis of recruited macrophages was also enhanced with UV/ozone irradiated titanium. Cytokines released from macrophages and the microenvironment purified by phagocytosis of macrophages contributed to the osteogenic activity of MSCs, fibroblasts, and angioblasts. The end result was an upregulated balance of bone remodeling and accelerated osteointegration of UV/ozone irradiated titanium biomaterials.

5. Conclusion

The success of bone regeneration is based on beneficial immune response against bacteria and coordinated cross-talk among MSCs. In the present study, we firstly developed three different cell and bacteria co-culture systems to investigate the race between macrophages and bacteria to adhere to surface of biomaterials. We proved that UV/ozone irradiation could significantly manipulate the immune response against *S. aureus* with excellent antibacterial activity and also generate a favorable osteoimmune microenvironment on titanium. These findings suggest that UV/ozone irradiation could be an excellent potential strategy to enhance bone biomaterials with the best functional outcomes dealing with both infection and inflammation conditions in clinical applications.

CRedit authorship contribution statement

Yuanyuan Yang: Writing – original draft, Investigation. **Honghao Zhang:** Conceptualization, Methodology, Writing – review & editing. **Satoshi Komasa:** Data curation, Formal analysis, Software, Project administration. **Yukihiro Morimoto:** Resources. **Tohru Sekino:**

Resources. **Takayoshi Kawazoe:** Supervision. **Joji Okazaki:** Funding acquisition, Project administration.

Declaration of competing interest

The authors declare that they have no known competing financial interests or personal relationships that could have appeared to influence the work reported in this paper.

Acknowledgements

The authors are grateful for the financial support from the Japan Society for the Promotion of Science (grant numbers: 20K18651, 19K05059). We are grateful to the members of the Department of Removable Prosthodontics and Occlusion for their kind advice and help. We thank Dr. Eisuke Domae, Department of Biochemistry, Osaka Dental University, for his valuable discussions. We also thank Dr. Kengo Iwasaki and Mr. Naoya Kawade from the Central Institute of Dental Research, Osaka Dental University, for his kind help with the experimental techniques.

Appendix A. Supplementary data

Supplementary data to this article can be found online at <https://doi.org/10.1016/j.msec.2021.112377>.

References

- [1] D.J. Hak, D. Fitzpatrick, J.A. Bishop, J.L. Marsh, S. Tilp, R. Schnettler, H. Simpson, V. Alt, Delayed union and nonunions: epidemiology, clinical issues, and financial aspects, *Injury* 45 (Suppl. 2) (2014) S3–S7, <https://doi.org/10.1016/j.injury.2014.04.002>.
- [2] A.G. Gristina, Biomaterial-centered infection: microbial adhesion versus tissue integration, *Science* 237 (1987) 1588–1595, <https://doi.org/10.1126/science.3629258>.
- [3] L. Tan, J. Li, X. Liu, Z. Cui, X. Yang, S. Zhu, Z. Li, X. Yuan, Y. Zheng, K.W.K. Yeung, H. Pan, X. Wang, S. Wu, Rapid biofilm eradication on bone implants using red phosphorus and near-infrared light, *Adv. Mater.* 30 (2018), e1801808, <https://doi.org/10.1002/adma.201801808>.
- [4] F. Loi, L.A. Córdova, J. Pajarinen, T.H. Lin, Z. Yao, S.B. Goodman, Inflammation, fracture and bone repair, *Bone* 86 (2016) 119–130, <https://doi.org/10.1016/j.bone.2016.02.020>.
- [5] O. Bastian, J. Pillay, J. Alblas, L. Leenen, L. Koenderman, T. Blokhuis, Systemic inflammation and fracture healing, *J. Leukoc. Biol.* 89 (2011) 669–673, <https://doi.org/10.1189/jlb.0810446>.
- [6] L.R. Thurlow, M.L. Hanke, T. Fritz, A. Angle, A. Aldrich, S.H. Williams, I. L. Engbrechtsen, K.W. Bayles, A.R. Horswill, T. Kielian, *Staphylococcus aureus* biofilms prevent macrophage phagocytosis and attenuate inflammation in vivo, *J. Immunol.* 186 (2011) 6585–6596, <https://doi.org/10.4049/jimmunol.1002794>.
- [7] J.D. Bryers, C.M. Giachelli, B.D. Ratner, Engineering biomaterials to integrate and heal: the biocompatibility paradigm shifts, *Biotechnol. Bioeng.* 109 (2012) 1898–1911, <https://doi.org/10.1002/bit.24559>.
- [8] J.M. Anderson, A. Rodriguez, D.T. Chang, Foreign body reaction to biomaterials, *Semin. Immunol.* 20 (2008) 86–100, <https://doi.org/10.1016/j.smim.2007.11.004>.
- [9] J.M. Anderson, J.A. Jones, Phenotypic dichotomies in the foreign body reaction, *Biomaterials* 28 (2007) 5114–5120, <https://doi.org/10.1016/j.biomaterials.2007.07.010>.
- [10] P.J. Murray, T.A. Wynn, Protective and pathogenic functions of macrophage subsets, *Nat. Rev. Immunol.* 11 (2011) 723–737, <https://doi.org/10.1038/nri3073>.
- [11] S. Gordon, P.R. Taylor, Monocyte and macrophage heterogeneity, *Nat. Rev. Immunol.* 5 (2005) 953–964, <https://doi.org/10.1038/nri1733>.
- [12] R.S. Flannagan, G. Cosío, G. Grinstein, Antimicrobial mechanisms of phagocytes and bacterial evasion strategies, *Nat. Rev. Microbiol.* 7 (2009) 355–366, <https://doi.org/10.1038/nrmicro2128>.
- [13] D.M. Mosser, J.P. Edwards, Exploring the full spectrum of macrophage activation, *Nat. Rev. Immunol.* 8 (2008) 958–969, <https://doi.org/10.1038/nri2448>.
- [14] C.J. Chen, H. Kono, D. Golenbock, G. Reed, S. Akira, K.L. Rock, Identification of a key pathway required for the sterile inflammatory response triggered by dying cells, *Nat. Med.* 13 (2007) 851–856, <https://doi.org/10.1038/nm1603>.
- [15] V. Thammavongsa, D.M. Missiakos, O. Schneewind, *Staphylococcus aureus* degrades neutrophil extracellular traps to promote immune cell death, *Science* 342 (2013) 863–866, <https://doi.org/10.1126/science.1242255>.
- [16] C.R. Ariola, D. Campoccia, L. Montanaro, Implant infections: adhesion, biofilm formation and immune evasion, *Nat. Rev. Microbiol.* 16 (2018) 397–409, <https://doi.org/10.1038/s41579-018-0019-y>.
- [17] A.E. Paharik, A.R. Horswill, The staphylococcal biofilm: adhesins, regulation, and host response, *Microbiol. Spectr.* 4 (2016) 2, <https://doi.org/10.1128/microbiolspec.VMBF-0022-2015>.
- [18] C.R. Ariola, D. Campoccia, P. Speziale, L. Montanaro, J.W. Costerton, Biofilm formation in *Staphylococcus* implant infections. A review of molecular mechanisms and implications for biofilm-resistant materials, *Biomaterials* 33 (2012) 5967–5982, <https://doi.org/10.1016/j.biomaterials.2012.05.031>.
- [19] M. Tsukasaki, H. Takayanagi, Osteoimmunology: evolving concepts in bone-immune interactions in health and disease, *Nat. Rev. Immunol.* 19 (2019) 626–642, <https://doi.org/10.1038/s41577-019-0178-8>.
- [20] K. Okamoto, T. Nakashima, M. Shinohara, T. Negishi-Koga, N. Komatsu, A. Terashima, S. Sawa, T. Nitta, H. Takayanagi, Osteoimmunology: the conceptual framework unifying the immune and skeletal systems, *Physiol. Rev.* 97 (2017) 1295–1349, <https://doi.org/10.1152/physrev.00036.2016>.
- [21] H. Takayanagi, Osteoimmunology: shared mechanisms and crosstalk between the immune and bone systems, *Nat. Rev. Immunol.* 7 (2007) 292–304, <https://doi.org/10.1038/nri2062>.
- [22] S.L. Teitelbaum, F.P. Ross, Genetic regulation of osteoclast development and function, *Nat. Rev. Genet.* 4 (2003) 638–649, <https://doi.org/10.1038/nrg1122>.
- [23] Z. Chen, T. Klein, R.Z. Murray, R. Crawford, J. Chang, C. Wu, Y. Xiao, Osteoimmunomodulation for the development of advanced bone biomaterials, *Mater. Today* 19 (2016), <https://doi.org/10.1016/j.mattod.2015.11.004> (304–321–s321).
- [24] B.N. Brown, B.D. Ratner, S.B. Goodman, S. Amar, S.F. Badylak, Macrophage polarization: an opportunity for improved outcomes in biomaterials and regenerative medicine, *Biomaterials* 33 (2012) 3792–3802, <https://doi.org/10.1016/j.biomaterials.2012.02.034>.
- [25] L. Vi, G.S. Baht, H. Whetstone, A. Ng, Q. Wei, R. Poon, S. Mylvaganam, M. Grynaps, B.A. Alman, Macrophages promote osteoblastic differentiation in-vivo: implications in fracture repair and bone homeostasis, *J. Bone Miner. Res.* 30 (2015) 1090–1102, <https://doi.org/10.1002/jbmr.2422>.
- [26] F.O. Martinez, A. Sica, A. Mantovani, M. Locati, Macrophage activation and polarization, *Front. Biosci.* 13 (2008) 453–461, <https://doi.org/10.2741/2692>.
- [27] Y. Zhang, T. Böse, R.E. Unger, J.A. Jansen, C.J. Kirkpatrick, J.J.P. van den Beucken, Macrophage type modulates osteogenic differentiation of adipose tissue MSCs, *Cell Tissue Res.* 369 (2017) 273–286, <https://doi.org/10.1007/s00441-017-2598-8>.
- [28] E. Gibon, F. Loi, L.A. Córdova, J. Pajarinen, T. Lin, L. Lu, A. Nabeshima, Z. Yao, S. B. Goodman, Aging affects bone marrow macrophage polarization: relevance to bone healing, *Regen. Eng. Transl. Med.* 2 (2016) 98–104, <https://doi.org/10.1007/s40883-016-0016-5>.
- [29] Y. Yin, R.X. Wu, X.T. He, X.Y. Xu, J. Wang, F.M. Chen, Influences of age-related changes in mesenchymal stem cells on macrophages during in-vitro culture, *Stem Cell Res. Ther.* 8 (2017) 153, <https://doi.org/10.1186/s13287-017-0608-0>.
- [30] G. Juban, B. Chazaud, Metabolic regulation of macrophages during tissue repair: insights from skeletal muscle regeneration, *FEBS Lett.* 591 (2017) 3007–3021, <https://doi.org/10.1002/1873-3468.12703>.
- [31] B.G. Keselowsky, D.M. Collard, A.J. Garcia, Surface chemistry modulates focal adhesion composition and signaling through changes in integrin binding, *Biomaterials* 25 (2004) 5947–5954, <https://doi.org/10.1016/j.biomaterials.2004.01.062>.
- [32] J. Yang, L.E. McNamara, N. Gadegaard, E.V. Alakpa, K.V. Burgess, R.M. Meek, M. J. Dalby, Nanotopographical induction of osteogenesis through adhesion, bone morphogenic protein cosignaling, and regulation of microRNAs, *ACS Nano* 8 (2014) 9941–9953, <https://doi.org/10.1021/nn504767g>.
- [33] G. Wang, W. Jin, A.M. Qasim, A. Gao, X. Peng, W. Li, H. Feng, P.K. Chu, Antibacterial effects of titanium embedded with silver nanoparticles based on electron-transfer-induced reactive oxygen species, *Biomaterials* 124 (2017) 25–34, <https://doi.org/10.1016/j.biomaterials.2017.01.028>.
- [34] B. Mehrjou, S. Mo, D. Dehghan-Baniani, G. Wang, A.M. Qasim, P.K. Chu, Antibacterial and cytocompatible nanoengineered silk-based materials for orthopedic implants and tissue engineering, *ACS Appl. Mater. Interfaces* 11 (2019) 31605–31614, <https://doi.org/10.1021/acsami.9b09066>.
- [35] W. Liu, J. Li, M. Cheng, Q. Wang, Y. Qian, K.W.K. Yeung, P.K. Chu, X. Zhang, A surface-engineered polyetheretherketone biomaterial implant with direct and immunoregulatory antibacterial activity against methicillin-resistant *Staphylococcus aureus*, *Biomaterials* 208 (2019) 8–20, <https://doi.org/10.1016/j.biomaterials.2019.04.008>.
- [36] T. Ueno, M. Yamada, T. Suzuki, H. Minamikawa, N. Sato, N. Hori, K. Takeuchi, M. Hattori, T. Ogawa, Enhancement of bone-titanium integration profile with UV-photofunctionalized titanium in a gap healing model, *Biomaterials* 31 (2010) 1546–1557, <https://doi.org/10.1016/j.biomaterials.2009.11.018>.
- [37] F. Iwasa, N. Hori, T. Ueno, H. Minamikawa, M. Yamada, T. Ogawa, Enhancement of osteoblast adhesion to UV-photofunctionalized titanium via an electrostatic mechanism, *Biomaterials* 31 (2010) 2717–2727, <https://doi.org/10.1016/j.biomaterials.2009.12.024>.
- [38] N. Tsukimura, M. Yamada, F. Iwasa, H. Minamikawa, W. Att, T. Ueno, L. Saruwatari, H. Aita, W.A. Chiou, T. Ogawa, Synergistic effects of UV photofunctionalization and micro-nano hybrid topography on the biological properties of titanium, *Biomaterials* 32 (2011) 4358–4368, <https://doi.org/10.1016/j.biomaterials.2011.03.001>.
- [39] E.D. de Avila, B.P. Lima, T. Sekiya, Y. Torii, T. Ogawa, W. Shi, R. Lux, Effect of UV-photofunctionalization on oral bacterial attachment and biofilm formation to titanium implant material, *Biomaterials* 67 (2015) 84–92, <https://doi.org/10.1016/j.biomaterials.2015.07.030>.
- [40] H. Zhang, S. Komasa, C. Mashimo, T. Sekino, J. Okazaki, Effect of ultraviolet treatment on bacterial attachment and osteogenic activity to alkali-treated titanium with nanonetwork structures, *Int. J. Nanomedicine* 12 (2017) 4633–4646, <https://doi.org/10.2147/IJN.S136273>.
- [41] H. Suzuki, K. Kasai, Y. Kimura, S. Miyata, UV/ozone surface modification combined with atmospheric pressure plasma irradiation for cell culture plastics to improve pluripotent stem cell culture, *Mater. Sci. Eng. C Mater. Biol. Appl.* 123 (2021) 112012, <https://doi.org/10.1016/j.msec.2021.112012>.
- [42] B.H. Kapadia, R.A. Berg, J.A. Daley, J. Fritz, A. Bhav, M.A. Mont, Periprosthetic joint infection, *Lancet.* 387 (2016) 386–394, [https://doi.org/10.1016/S0140-6736\(14\)61798-0](https://doi.org/10.1016/S0140-6736(14)61798-0).
- [43] H.J. Busscher, H.C. van der Mei, G. Subbiahdoss, P.C. Jutte, J.J. van den Dungen, S. A. Zaai, M.J. Schultz, D.W. Grainger, Biomaterial-associated infection: locating the finish line in the race for the surface, *Sci. Transl. Med.* 4 (2012), 153rv10, <https://doi.org/10.1126/scitranslmed.3004528>.
- [44] S.N. Abraham, Y. Miao, The nature of immune responses to urinary tract infections, *Nat. Rev. Immunol.* 15 (2015) 655–663, <https://doi.org/10.1038/nri3887>.
- [45] Y. Zhao, C. Ye, W. Liu, R. Chen, X. Jiang, Tuning the composition of AuPt bimetallic nanoparticles for antibacterial application, *Angew. Chem. Int. Ed. Engl.* 53 (2014) 8127–8131, <https://doi.org/10.1002/anie.201401035>.
- [46] Y. Tao, E. Ju, J. Ren, X. Qu, Bifunctionalized mesoporous silica-supported gold nanoparticles: intrinsic oxidase and peroxidase catalytic activities for antibacterial applications, *Adv. Mater.* 27 (2015) 1097–1104, <https://doi.org/10.1002/adma.201405105>.
- [47] Z. Fan, B. Liu, J. Wang, S. Zhang, Q. Lin, P. Gong, L. Ma, S. Yang, A novel wound dressing based on Ag/graphene polymer hydrogel: effectively kill bacteria and accelerate wound healing, *Adv. Funct. Mater.* 24 (2014) 3933–3943, <https://doi.org/10.1002/adfm.201304202>.

- [48] J. Wang, J. Li, G. Guo, Q. Wang, J. Tang, Y. Zhao, H. Qin, T. Wahafu, H. Shen, X. Liu, X. Zhang, Silver-nanoparticles-modified biomaterial surface resistant to staphylococcus: new insight into the antimicrobial action of silver, *Sci. Rep.* 6 (2016) 32699, <https://doi.org/10.1038/srep32699>.
- [49] W. Liu, J. Li, M. Cheng, Q. Wang, K.W.K. Yeung, P.K. Chu, X. Zhang, Zinc-modified sulfonated polyetheretherketone surface with immunomodulatory function for guiding cell fate and bone regeneration, *Adv. Sci. (Weinh)* 5 (2018), 1800749, <https://doi.org/10.1002/advs.201800749>.
- [50] M.J. Hajipour, K.M. Fromm, A.A. Ashkarran, D. Jimenez de Aberasturi, I.R. de Laramendi, T. Rojo, V. Serpooshan, W.J. Parak, M. Mahmoudi, Antibacterial properties of nanoparticles, *Trends Biotechnol.* 30 (2012) 499–511, <https://doi.org/10.1016/j.tibtech.2012.06.004>.
- [51] D. Campoccia, L. Montanaro, C.R. Arciola, A review of the biomaterials technologies for infection-resistant surfaces, *Biomaterials* 34 (2013) 8533–8554, <https://doi.org/10.1016/j.biomaterials.2013.07.089>.
- [52] W.H. De Jong, L.T. Van Der Ven, A. Sleijffers, M.V. Park, E.H. Jansen, H. Van Loveren, R.J. Vandebriel, Systemic and immunotoxicity of silver nanoparticles in an intravenous 28 days repeated dose toxicity study in rats, *Biomaterials* 34 (2013) 8333–8343, <https://doi.org/10.1016/j.biomaterials.2013.06.048>.
- [53] D. Mao, F. Hu, S. Ji Kenry, W. Wu, D. Ding, D. Kong, B. Liu, Metal-organic-framework-assisted in vivo bacterial metabolic labeling and precise antibacterial therapy, *Adv. Mater.* 30 (2018), e1706831, <https://doi.org/10.1002/adma.201706831>.
- [54] E.M. Schwarz, S.L. Kates, V. Alt, The 1st international consensus meeting on periprosthetic joint infection, in: *J. Orthop. Res.* 1st International Consensus Meeting on Periprosthetic Joint Infection. 32. Suppl 1, 2014, p. S1, <https://doi.org/10.1002/jor.22542>.
- [55] M.T. Silva, Macrophage phagocytosis of neutrophils at inflammatory/infectious foci: a cooperative mechanism in the control of infection and infectious inflammation, *J. Leukoc. Biol.* 89 (2011) 675–683, <https://doi.org/10.1189/jlb.0910536>.
- [56] K.M. Rigby, F.R. DeLeo, Neutrophils in innate host defense against *Staphylococcus aureus* infections, *Semin. Immunopathol.* 34 (2012) 237–259, <https://doi.org/10.1007/s00281-011-0295-3>.
- [57] G.D. Fairn, S. Grinstein, How nascent phagosomes mature to become phagolysosomes, *Trends Immunol.* 33 (2012) 397–405, <https://doi.org/10.1016/j.it.2012.03.003>.
- [58] K. Kasai, Y. Kimura, S. Miyata, Improvement of adhesion and proliferation of mouse embryonic stem cells cultured on ozone/UV surface-modified substrates, *Mater. Sci. Eng. C Mater. Biol. Appl.* 78 (2017) 354–361, <https://doi.org/10.1016/j.msec.2017.04.021>.
- [59] A.G. Gristina, P. Naylor, Q. Myrvik, Infections from biomaterials and implants: a race for the surface, *Med. Prog. Technol.* 14 (1988–1989) 205–224. (PMID: 2978593).
- [60] M. Hindié, D. Wu, K. Anselme, O. Gallet, P. Di Martino, Effects of fibronectin coating on bacterial and osteoblast progenitor cells adherence in a co-culture assay, *Adv. Exp. Med. Biol.* 973 (2017) 17–30, https://doi.org/10.1007/5584_2016_41.
- [61] R. Trindade, T. Albrektsson, P. Tengvall, A. Wennerberg, Foreign body reaction to biomaterials: on mechanisms for buildup and breakdown of osseointegration, *Clin. Implant Dent. Relat. Res.* 18 (2016) 192–203, <https://doi.org/10.1111/cid.12274>.
- [62] O. Takeuchi, S. Akira, Pattern recognition receptors and inflammation, *Cell* 140 (2010) 805–820, <https://doi.org/10.1016/j.cell.2010.01.022>.
- [63] N. Parameswaran, S. Patial, Tumor necrosis factor- α signaling in macrophages, *Crit. Rev. Eukaryot. Gene Expr.* 20 (2010) 87–103, <https://doi.org/10.1615/critrevukargeneexpr.v20.i2.10>.
- [64] T. Hanada, A. Yoshimura, Regulation of cytokine signaling and inflammation, *Cytokine Growth Factor Rev.* 13 (2002) 413–421, [https://doi.org/10.1016/s1359-6101\(02\)00026-6](https://doi.org/10.1016/s1359-6101(02)00026-6).
- [65] A. Haschemi, P. Kosma, L. Gille, C.R. Evans, C.F. Burant, P. Starkl, B. Knapp, R. Haas, J.A. Schmid, C. Jandl, S. Amir, G. Lubec, J. Park, H. Esterbauer, M. Bilban, L. Brizuela, J.A. Pospisilik, L.E. Otterbein, O. Wagner, The sedoheptulose kinase CARL directs macrophage polarization through control of glucose metabolism, *Cell Metab.* 15 (2012) 813–826, <https://doi.org/10.1016/j.cmet.2012.04.023>.
- [66] R.B. Hamanaka, A. Glasauer, P. Hoover, S. Yang, H. Blatt, A.R. Mullen, S. Getsios, C.J. Gottardi, R.J. DeBerardinis, R.M. Lavker, N.S. Chandel, Mitochondrial reactive oxygen species promote epidermal differentiation and hair follicle development, *Sci. Signal.* 6 (2013) ra8, <https://doi.org/10.1126/scisignal.2003638>.
- [67] S. Salzano, P. Checconi, E.M. Hanschmann, C.H. Lillig, L.D. Bowler, P. Chan, D. Vaudry, M. Mengozzi, L. Coppo, S. Sacre, K.R. Atkuri, B. Sahaf, L.A. Herzenberg, L.A. Herzenberg, L. Mullen, P. Ghezzi, Linkage of inflammation and oxidative stress via release of glutathionylated peroxiredoxin-2, which acts as a danger signal, *Proc. Natl. Acad. Sci. U. S. A.* 111 (2014) 12157–12162, <https://doi.org/10.1073/pnas.1401712111>.
- [68] P. Ghezzi, Role of glutathione in immunity and inflammation in the lung, *Int. J. Gen. Med.* 4 (2011) 105–113, <https://doi.org/10.2147/IJGM.S15618>.
- [69] H. Kamata, S. Honda, S. Maeda, L. Chang, H. Hirata, M. Karin, Reactive oxygen species promote TNF α -induced death and sustained JNK activation by inhibiting MAP kinase phosphatases, *Cell* 120 (2005) 649–661, <https://doi.org/10.1016/j.cell.2004.12.041>.
- [70] A. El-Kenawi, B. Ruffell, Inflammation, ROS, and mutagenesis, *Cancer Cell* 32 (2017) 727–729, <https://doi.org/10.1016/j.ccell.2017.11.015>.
- [71] S. Vukicevic, L. Grgurevic, BMP-6 and mesenchymal stem cell differentiation, *Cytokine Growth Factor Rev.* 20 (2009) 441–448, <https://doi.org/10.1016/j.cytogr.2009.10.020>.
- [72] V. Nicolaïdou, M.M. Wong, A.N. Redpath, A. Ersek, D.F. Baban, L.M. Williams, A. P. Cope, N.J. Horwood, Monocytes induce STAT3 activation in human mesenchymal stem cells to promote osteoblast formation, *PLoS One* 7 (2012), e39871, <https://doi.org/10.1371/journal.pone.0039871>.
- [73] P. Guihard, Y. Danger, B. Brounais, E. David, R. Brion, J. Delecir, C.D. Richards, S. Chevalier, F. Rédini, D. Heymann, H. Gascan, F. Blanchard, Induction of osteogenesis in mesenchymal stem cells by activated monocytes/macrophages depends on oncostatin M signaling, *Stem Cells* 30 (2012) 762–772, <https://doi.org/10.1002/stem.1040>.
- [74] H. Takayanagi, New developments in osteoimmunology, *Nat. Rev. Rheumatol.* 8 (2012) 684–689, <https://doi.org/10.1038/nrrheum.2012.167>.
- [75] T. Kawai, S. Akira, The role of pattern-recognition receptors in innate immunity: update on toll-like receptors, *Nat. Immunol.* 11 (2010) 373–384, <https://doi.org/10.1038/ni.1863>.
- [76] A. Aderem, R.J. Ulevitch, Toll-like receptors in the induction of the innate immune response, *Nature* 406 (2000) 782–787, <https://doi.org/10.1038/35021228>.
- [77] T. Perlot, J.M. Penninger, Development and function of murine B cells lacking RANK, *J. Immunol.* 188 (2012) 1201–1205, <https://doi.org/10.4049/jimmunol.1102063>.
- [78] W.C. Dougall, M. Glaccum, K. Charrier, K. Rohrbach, K. Brasel, T. De Smedt, E. Daro, J. Smith, M.E. Tometsko, C.R. Maliszewski, A. Armstrong, V. Shen, S. Bain, D. Cosman, D. Anderson, P.J. Morrissey, J.J. Peschon, J. Schuh, RANK is essential for osteoclast and lymph node development, *Genes Dev.* 13 (1999) 2412–2424, <https://doi.org/10.1101/gad.13.18.2412>.
- [79] Y.Y. Kong, H. Yoshida, I. Sarosi, H.L. Tan, E. Timms, C. Capparelli, S. Morony, A. J. Oliveira-dos-Santos, G. Van, A. Itie, W. Khoo, A. Wakeham, C.R. Dunstan, D. L. Lacey, T.W. Mak, W.J. Boyle, J.M. Penninger, OPGL is a key regulator of osteoclastogenesis, lymphocyte development and lymph-node organogenesis, *Nature* 397 (1999) 315–323, <https://doi.org/10.1038/16852>.
- [80] D. Toben, I. Schroeder, T. El Khassawna, M. Mehta, J.E. Hoffmann, J.T. Frisch, H. Schell, J. Lienau, A. Serra, A. Radbruch, G.N. Duda, Fracture healing is accelerated in the absence of the adaptive immune system, *J. Bone Miner. Res.* 26 (2011) 113–124, <https://doi.org/10.1002/jbmr.185>.
- [81] G.E. Glass, J.K. Chan, A. Freidin, N. Feldmann, N.J. Horwood, J. Nanchahal, TNF- α promotes fracture repair by augmenting the recruitment and differentiation of muscle-derived stromal cells, *Proc. Natl. Acad. Sci. U. S. A.* 108 (2011) 1585–1590, <https://doi.org/10.1073/pnas.1018501108>.
- [82] J. Alblowi, R.A. Kayal, M. Siqueira, E. McKenzie, N. Krothapalli, J. McLean, J. Conn, B. Nikolajczyk, T.A. Einhorn, L. Gerstenfeld, D.T. Graves, High levels of tumor necrosis factor- α contribute to accelerated loss of cartilage in diabetic fracture healing, *Am. J. Pathol.* 175 (2009) 1574–1585, <https://doi.org/10.2353/ajpath.2009.090148>.
- [83] H. Huang, N. Zhao, X. Xu, Y. Xu, S. Li, J. Zhang, P. Yang, Dose-specific effects of tumor necrosis factor alpha on osteogenic differentiation of mesenchymal stem cells, *Cell Prolif.* 44 (2011) 420–427, <https://doi.org/10.1111/j.1365-2184.2011.00769.x>.
- [84] M.H.A. Abdel Meguid, Y.H. Hamad, R.S. Swilam, M.S. Barakat, Relation of interleukin-6 in rheumatoid arthritis patients to systemic bone loss and structural bone damage, *Rheumatol. Int.* 33 (2013) 697–703, <https://doi.org/10.1007/s00296-012-2375-7>.